Department of

APPLIED MATHEMATICS

NUMERICAL SOLUTION OF THE BUCKLEY-LEVERETT EQUATION WITH A GENERAL FRACTIONAL FLOW FUNCTION

by

Øystein Pettersen

Report no. 76 November 1984

UNIVERSITY OF BERGEN

Bergen, Norway

Department of Mathematics
University of Bergen
5000 Bergen, Norway

ISSN-0084-778X

NUMERICAL SOLUTION OF THE BUCKLEY-LEVERETT EQUATION WITH A GENERAL FRACTIONAL FLOW FUNCTION

by

Øystein Pettersen

Report no. 76 November 1984

Abstract

A dispersion-free numerical procedure for the solution of nonlinear conservation equations based on exact solutions of the Riemann Problem by the Random Choice Method is reviewed. This paper is concentrated on the displacement of oil by water in a onedimensional porous rock, however, the technique applies equally well to a variety of physical problems where accurate modelling of the evolution of discontinuities/shock waves is imperative.

For immiscible displacement, the nonlinear part of the conservation equation is an empirical function with error bounds. The effect of representing the (unknown) smooth nonlinearity function by a tabulated version is studied, accompanied with a proof for the structural stability of the problem with respect to small perturbations in the nonlinear function.

1 Introduction

The Buckley-Leverett Equation of reservoir dynamics is a special case of a non-linear conservation equation. The development of discontinuities that such equations permit, traditionally has been difficult to describe numerically by finite difference methods, as the discontinuities (shock fronts) inevitably are smoothened by the FDE algorithm (numerical dispersion).

Based on a work by Glimm[7], several authors have contributed to the development of a numerical procedure where the analytical solution of the Riemann problem is used to construct a global solution which is free for numerical dispersion. (See references at end of paper.) The positions of the shock fronts are computed without error, and the method is close to being second order accurate. A thorough description of the method is given in the first part of the text.

The nonlinear part of the Buckley-Leverett Equation is basically a function of the mobility ratio of the two fluids present. This ratio is virtually an empirical function of the wetting fluid saturation. Previous authors have, however, assumed a given analytical dependence on saturation in their works. We generalize the method by allowing the fractional flow function to be given by empirical table values. Inaccurate measurements introduce sources of error into the description of the nonlinearity function. The method therefore must be structurally stable with respect to perturbations in this function, a demand which we will show is fulfilled.

Another extension of previous theory is that, restricted to physical possible situations, we permit the nonlinear function to have a quite general shape.

The problem will be studied in one dimension only, for applications in multidimensional problems we refer to the list of references.

2 **Basic Equations**

Our object shall be the description of one-dimensional flow of two immiscible and incompressible fluids (water and oil). Sources and sinks are located only at the boundary of the model, and will be described by the boundary conditions, not included in the governing equations.

The basic equations are:

$$(1) \quad \frac{\partial u_i}{\partial x} + \Phi(x)\frac{\partial S_i}{\partial t} = 0 \qquad \text{(Continuity Equation)}$$

$$(2) \quad u_i = -\frac{K(x)k_{ri}(S_i)}{\mu_i}\left\{\frac{\partial p_i}{\partial x} - \rho_i g\cos\theta\right\} \qquad \text{(Darcy's law)}$$

$$(3) \quad S_w + S_o = 1 \qquad \text{(Completely saturated rock.)}$$

$$(4) \quad p_c = p_c(S_w) = p_o - p_w \qquad \text{(Capillary Pressure Equation)}$$

In these equations subscript i denotes the two phases o (oil) and w (water), u_i is the Darcy velocity, S_i denotes saturation, K the rock permeability and k_{ri} relative permeability. p_c is the capillary pressure, Φ = rock porosity, ρ = density, g = gravity, μ = viscosity, and θ is the angle between the positive x-axis and the gravity vector.

We define the mobility of phase i by $\lambda_i = k_{ri}/\mu_i$ and the specific gravity by $\gamma_i = \rho_i g$.

Let $S = S_w$ (hence $S_o = 1 - S$ by Eq. (3)), and $p = p_w$.

Equations (1)-(4) are then written:

$$(5)\quad u_w = -K\lambda_w\left\{\frac{\partial p}{\partial x} - \gamma_w\cos\theta\right\}$$

$$(6)\quad u_o = -K\lambda_o\left\{\frac{\partial p}{\partial x} + \frac{\partial p_c}{\partial x} - \gamma_o\cos\theta\right\}$$

$$(7)\quad \frac{\partial u_w}{\partial x} + \Phi(x)\frac{\partial S}{\partial t} = 0$$

$$(8)\quad \frac{\partial u_o}{\partial x} - \Phi(x)\frac{\partial S}{\partial t} = 0$$

If we introduce the total Darcy velocity $u = u_w + u_o$, we see from Eqs. (7) and (8) that u is constant.
From Eqs. (5) and (6) we have:

$$(9)\quad u = -K\left[\!\left[(\lambda_w + \lambda_o)\frac{\partial p}{\partial x} - (\lambda_w\gamma_w + \lambda_o\gamma_o)\cos\theta + \lambda_o\frac{\partial p_c}{\partial x}\right]\!\right]$$

which gives the Pressure Equation:

$$(10)\quad \frac{\partial}{\partial x}\left\{K\cdot(\lambda_w + \lambda_o)\frac{\partial p}{\partial x}\right\} = \frac{\partial}{\partial x}K\cdot(\lambda_w\gamma_w + \lambda_o\gamma_o)\cos\theta - \frac{\partial}{\partial x}K\cdot\lambda_o\frac{\partial p_c}{\partial x}$$

By solving Eq. (9) with respect to the pressure gradient, combining Eqs. (5) and (7), and inserting the expression for the pressure gradient, we arrive at:

$$(11)\quad \frac{\partial}{\partial x}\left\{\frac{\lambda_w}{\lambda_w + \lambda_o}u + \frac{K\lambda_w\lambda_o}{\lambda_w + \lambda_o}\left[\!\left[\frac{\partial p_c}{\partial x} - (\gamma_o - \gamma_w)\cos\theta\right]\!\right]\right\} + \Phi\frac{\partial S}{\partial t} = 0$$

Denoting the derivative with respect to S by a dash, Eq. (11) can be expressed as:

$$(12)\quad \frac{\partial}{\partial x}\left\{ K\frac{\lambda_w\lambda_o}{\lambda_w+\lambda_o}p_c'(S)\frac{\partial S}{\partial x}\right\} +$$

$$+\left\{ \left[\!\left[\frac{\lambda_w}{\lambda_w+\lambda_o}\right]\!\right]' u + K(\gamma_o-\gamma_w)\cos\theta\left[\!\left[\frac{\lambda_w\lambda_o}{\lambda_w+\lambda_o}\right]\!\right]' \right\}\frac{\partial S}{\partial x} +$$

$$+(\gamma_o-\gamma_w)\cos\theta\frac{\lambda_w\lambda_o}{\lambda_w+\lambda_o}\frac{\partial K}{\partial x}+\Phi\frac{\partial S}{\partial t}=0$$

Equation (12) is known as the Saturation Equation.

We now assume that the rock is homogeneous, that u is time independent, and that capillary pressure is negligible.
Under these assumptions Eq. (12) is reduced to the well-known Buckley-Leverett Equation:

$$(13)\quad \frac{\partial S}{\partial t}+\frac{u}{\Phi}\frac{d}{dS}\left[\!\left[\frac{\lambda_w}{\lambda_w+\lambda_o}\left(1+\frac{K}{u}(\gamma_o-\gamma_w)\lambda_o\cos\theta\right)\right]\!\right]\frac{\partial S}{\partial x}=0$$

Equation (13) is a special case of the conservation equation:

$$(14)\quad \frac{\partial S}{\partial t}+\frac{\partial f(S)}{\partial x}=0$$

The nonlinearity function f(S) defined by Eq. (13) is known as the fractional flow function. We shall study Eq. (14) for a general nonlinearity function in the following.

3 The Riemann problem

In this section we will examine the properties of the solutions of the nonlinear hyperbolic conservation equation for a special initial condition. We use u as the dependent variable and denote differentials by subscripts. The model problem is then:

(15) $u_t + f(u)_x = 0$

(16) $u_0 = u(t=0) = \begin{cases} u_L, & x<0 \\ u_R, & x\geq 0 \end{cases}$

where u_L and u_R are constant cases.

The initial value problem (15)-(16) is known as the Riemann problem.

By defining $a(u) = \frac{\partial f}{\partial u}$, equation (15) may be written:

(17) $u_t + a(u)u_x = 0$

The linear case (a = pos. const.) has the solution:

(18) $u = \begin{cases} u_L, & x<at \\ u_R, & x\geq at \end{cases}$

i.e. a discontinuity moving to the right with the velocity a = dx/dt. In the x-t plane the solution is composed by two constant cases separated by the discontinuity line x = at. (Fig. 1.)

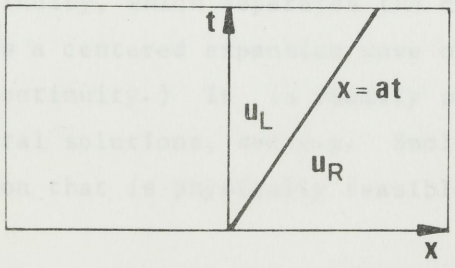

Fig. 1

Returning to the general case, we note that if u_0 = const., $u = u_0$ is a global solution of the Riemann problem.

For large positive x we hence may infer that the solution of the problem for small times is a wave $u = u_R$ propagating with a velocity $a(u_R)$, and for large negative x we will have a wave $u = u_L$ propagating

t
x=at
u^L
u^R
x

with a velocity $a(u_L)$.

These modes are, however, valid only for a limited time, depending on the absolute magnitude of x. As t increases or/and x approaches zero, this simple approach ceases to be valid. When $a(u_R) < a(u_L)$ the solution will become multiple-valued in finite time. (Fig. 2a)

The case $a(u_R) > a(u_L)$ implies that a sector expanding from the origin exists where no solution is defined. (Fig. 2b)

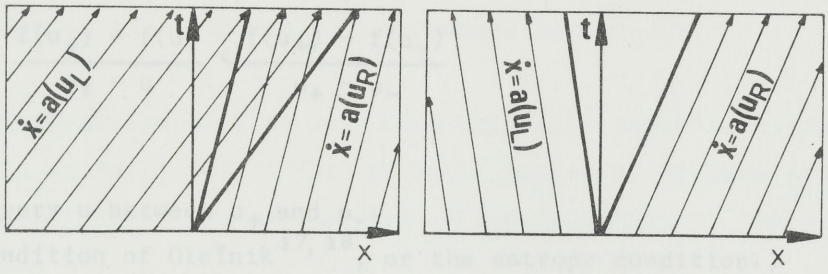

a) b)

Fig. 2

The Riemann problem has been intensively studied the last few decades, leading to a theoretical basis which can be looked upon as complete for one case, namely when f(u) is strict nonlinear, i.e. $a'(u) \neq 0$ for all u. The main contributors to the theory are Glimm et al, Lax, and Oleĭnik.

A complete description is found in e.g. Smoller[21].

We shall present a brief summary of the main results:

When $u_L \neq u_R$ we have a jump discontinuity at the origin of the x-t system. This discontinuity, which seperates the constant states u_L and u_R, will propagate as a centered expansion wave or a shock (which may be a contact discontinuity.) It is readily shown that the Riemann problem permits several solutions, see e.g. Smoller[21]. We seek the unique weak solution that is physically feasible. Then the following must hold:

Let $x = x(t)$ be a curve of discontinuity for a solution $u(x,t)$ of the Riemann problem. Let u_- be the limiting value of u as $x(t)$ is approached from the left, and $u_+ = \lim u(x,t)$ as x tends to $x(t)$ from the right. Standard shock theory then provides:

1) The curve of discontinuity is a straight line with slope

$$(19)\quad S_{+-} = \frac{dx}{dt} = \frac{f(u_+) - f(u_-)}{u_+ - u_-}$$

(Rankine-Huginot jump condition)

2)

$$(20)\quad \frac{f(u_+) - f(u)}{u_+ - u} \leq \frac{f(u_+) - f(u_-)}{u_+ - u_-}$$

for every u between u_+ and u_-.
(E-condition of Oleĭnik[17, 18], or the entropy condition.)

If u_1 and u_2 are two arbitrary values of u, we define

$$S_{12} = \frac{f(u_1) - f(u_2)}{u_1 - u_2}$$

as the slope of the straight line connecting the two points $(u_1, f(u_1))$ and $(u_2, f(u_2))$. The entropy condition then reads:

$S_{+,\cdot} \leq S_{+,-}$ for every u between u_+ and u_-.

If conditions (19) and (20) are not fulfilled, the appropriate solution must be continuous. Contrary to the linear case we here have a situation where discontinuous initial data may generate a smooth solution. On the other hand, discontinuities (shocks) can develop from smooth initial data.

Having described the conditions under which shocks are permitted to develop, we turn to the smooth solution case.
The situation is depicted in Fig. 2b. The two constant cases u_L and u_R are seperated by a region where for the time being no solution is defined. Looking at the physics, we have two waves propagating in the same direction, where the "first" wave has a greater velocity than the "second" one. In other words: The "first" wave is "running away" from the "second" one. This leads to the definition of the so-called

rarefaction wave. This wave is implemented as a smooth curve connecting the two constant states, so that the total solution is continuous.

More accurately: The sector that separates the constant states u_L and u_R is bounded by the straight lines $x = a_L \cdot t$ and $x = a_R \cdot t$, where $a_L = a(u_L)$ and $a_R = a(u_R)$.

We seek the rarefaction solution for $t = \tau > 0$ at a point $x = \xi$ within the sector. The desired solution is then $u(\tau,\xi) = a^{-1}(\xi)$. As ξ runs from a_R to a_L along the line segment $t = \tau$ inside the sector, we see indeed that the solution is everywhere continuous.

From the analysis so far, we conclude that only four permitted cases can exist as solutions of the strictly nonlinear Riemann problem. We shall denote these cases as the four primitive modes of the problem:

Mode 1: f(u) convex and $u_L > u_R$. (Rarefaction)
Mode 2: f(u) convex and $u_L < u_R$. (Shock)
Mode 3: f(u) concave and $u_L > u_R$. (Shock)
Mode 4: f(u) concave and $u_L < u_R$. (Rarefaction)

The primitive modes are shown pictorially in Figs. 3-6, where a) shows the nonlinearity function, b) the solution in the x-t plane, and c) is a qualitative picture of the solution along the line $t = \tau$.

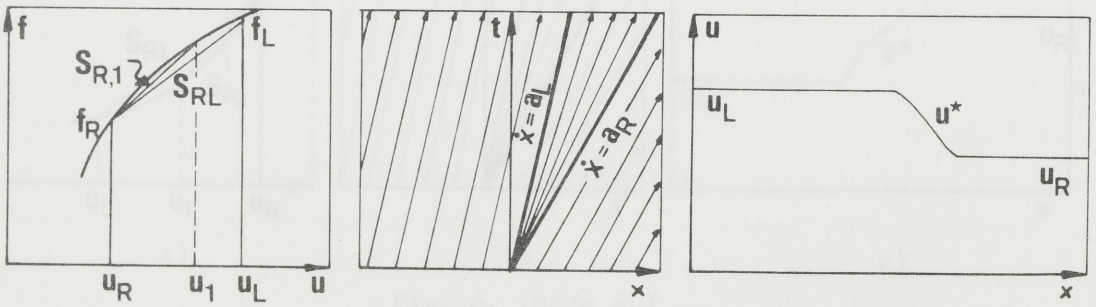

a) b) c)

Fig. 3. (Mode 1.)

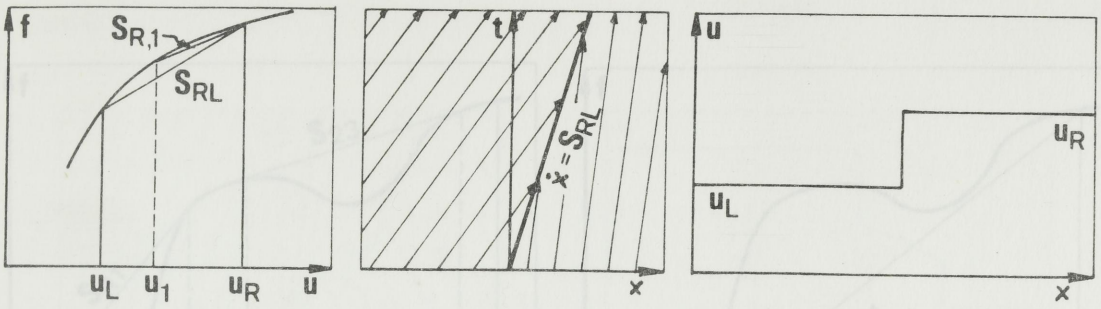

a) b) c)

Fig. 4. (Mode 2.)

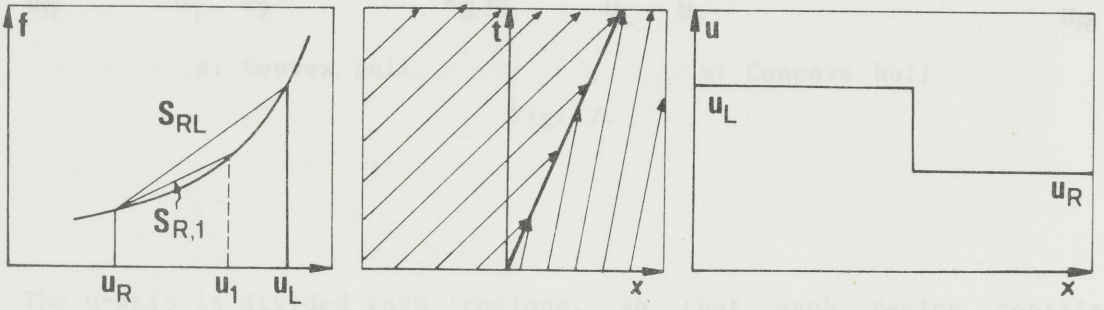

a) b) c)

Fig. 5. (Mode 3.)

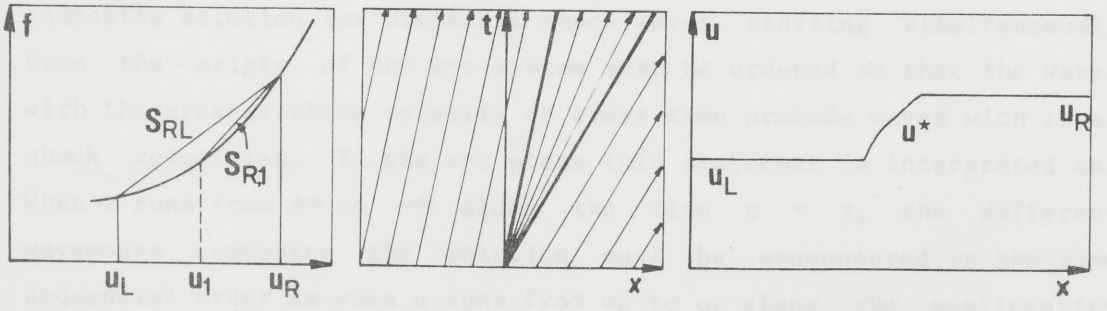

a) b) c)

Fig. 6. (Mode 4.)

Composite solutions.

When the condition of strict nonlinearity is violated, the solution is composed by several of the primitive modes. This case lacks the solid theoretical foundation that supplies the strict nonlinear case, but by physical reasoning and application of the conditions (19) and (20), it is possible to construct a solution that is unique and physically

acceptable. Fig. 7 shows a rather complex nonlinearity function.

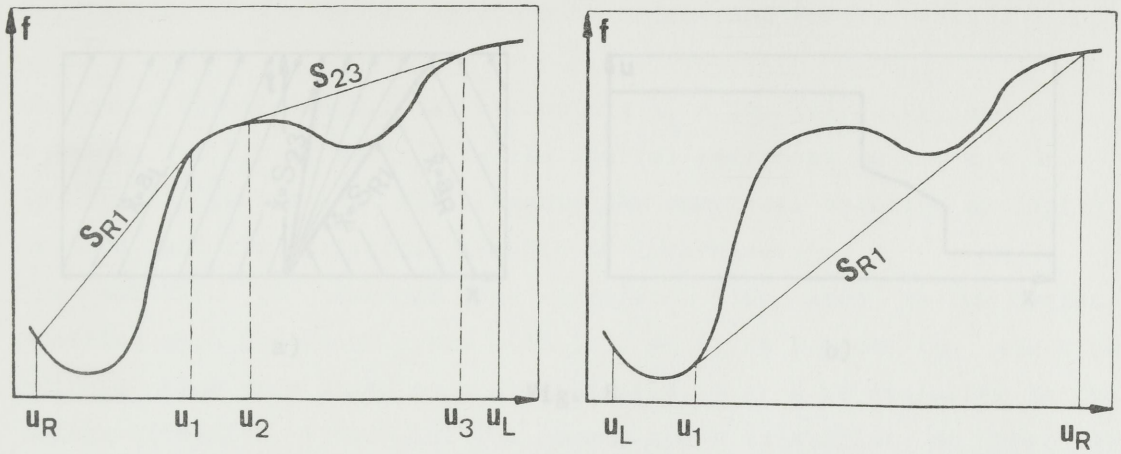

a: Convex hull b: Concave hull

Fig. 7.

The u-axis is divided into regions, so that each region contains exactly one primitive mode. From the E-condition we deduce that the classification into primitive modes always starts at the u_R-end of the diagram. The physical statement we use as basis for constructing the composite solution is: Different shock waves starting simultaneously from the origin of the x-t system must be ordered so that the waves with the greater shock velocity at every time precede waves with lower shock velocities. In the x-t plane this statement is interpreted as: When x runs from $+\infty$ to $-\infty$ along the line $t = \tau$, the different wavemodes composing the solution must be encountered in the same sequential order as when u runs from u_R to u_L along the nonlinearity function. I.e. the shock speeds must form a decreasing sequence when u varies as mentioned.

This request is satisfied if (and only if) we replace f(u) by its convex hull when $u_R < u_L$, and the concave hull if $u_L < u_R$. This procedure is based on a result by Harten[15], namely that the solution is independent of the actual shape of the nonlinearity function in the concave (convex) regions when $u_R < (>)\ u_L$.

The construction of the composite wave is then a simple task. The case shown in Fig. 7a will as an example be composed by a constant state u_R, a shock wave separating u_R from u_1, a rarefaction wave connecting

u_1 and u_2, and so on, resulting in a solution which is qualitatively shown in Fig. 8.

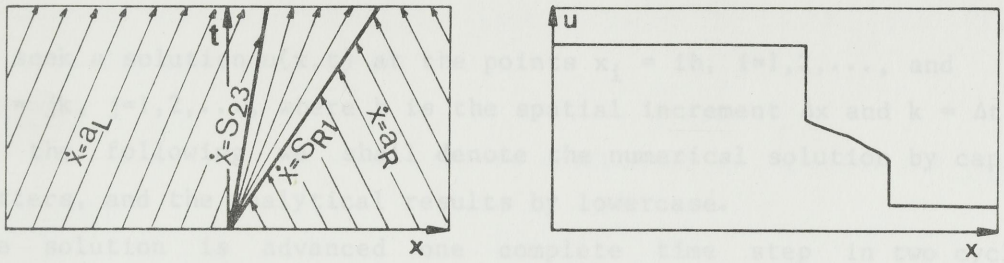

a) b)

Fig. 8

The solution corresponding to Fig. 7b is shown in Fig. 9:

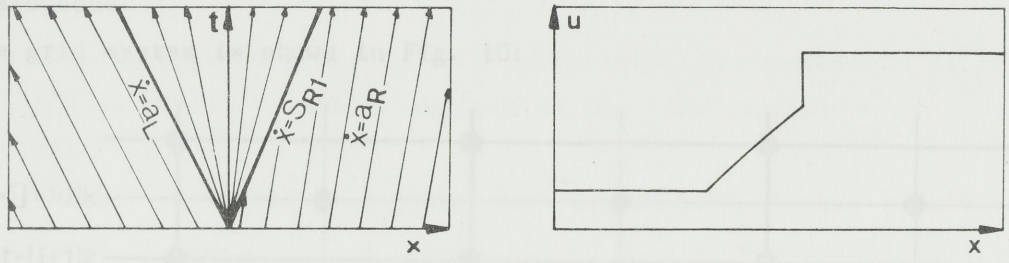

a) b)

Fig. 9

4 The Random Choice Method.

We now turn to the actual problem we are attempting to solve, namely:

$$(21) \quad u_t + f(u)_x = 0$$

$$(22) \quad u(t=0) = I(x)$$

$$(23) \quad u(x=0) = B_0(t), \qquad u(x=1) = B_1(t)$$

A method developed by Glimm[7] to prove the existence and boundedness of solutions to the Riemann problem, was during the 70´s used in a constructive manner to obtain a numerical solution to the problem

(21)-(23). The procedure has been developed and studied by Glimm, Marchesin, McBryan, Chorin and others[1-5, 7-13, 16, 20]. An excellent description of the method is given by Concus and Proskurowski[4].

We seek a solution $u(x,t)$ at the points $x_i = ih$, $i=1,2,\ldots$, and $t_j = jk$, $j=1,2,\ldots$, where h is the spatial increment Δx and $k = \Delta t$. In the following we shall denote the numerical solution by capital letters, and the analytical results by lowercase.

The solution is advanced one complete time step in two cycles. Starting with the known array $U(ih,jk)$, we first compute the solution half a time step ahead on a shifted grid, i.e. U is evaluated in the points $\{(i+1/2)h, (j+1/2)k\}$. The second cycle is similar, so that at the end of a complete time step, we obtain $U\{ih, (j+1)k\}$. In the following we concentrate on the first time cycle, the other half is analogeous.

The grid system is shown in Fig. 10:

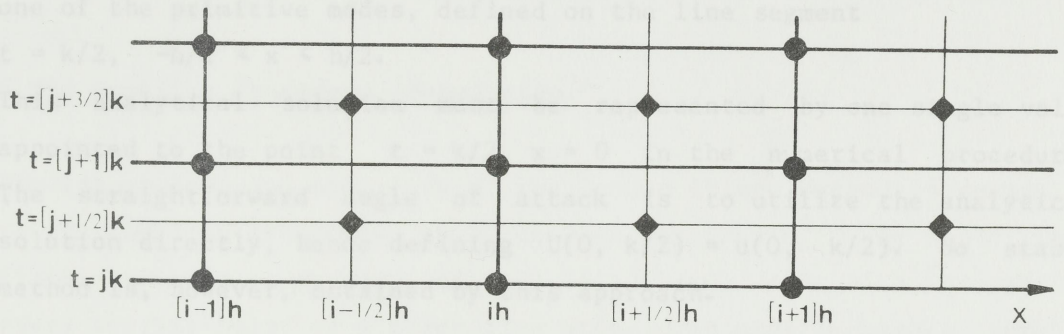

Fig. 10.

We use a control volume interpretation of the discrete approximation, i.e. $U(x,jk)$ is taken as constant on each interval $(i-1/2)h \leq x \leq (i+1/2)h$, and similar for $U\{x,(j+1/2)k\}$.

For the grid points (ih,jk) and $\{(i+1)h,jk\}$ we thus have the problem:

$$(24)\quad u_t + f(u)_x = 0 \qquad t \geq jk$$

$$(25)\quad U(t=jk) = \begin{cases} U(ih,jk), & x \leq (i+1/2)h \\ U\{(i+1)h,jk\}, & x > (i+1/2)h \end{cases}$$

In order to simplify both the notation and the computer programs, we shift the point $\{(i+1/2)h, jk\}$ to the origin. The original Riemann problem is then recognized. Our task is hence to solve one Riemann problem for each grid point.

If the size of the time step is restricted by imposing the Courant condition:

$$\max |a(u)| < h/k \tag{26}$$

we are guaranteed that none of the separate Riemann problems will interfer with each other, hence assuring that waves propagated from the discontinuity of different Riemann problems do not intersect.

The Riemann problem generates a complex solution composed of at least one of the primitive modes, defined on the line segment
$t = k/2, \quad -h/2 \leq x \leq h/2.$
This analytical solution must be represented by one single value appointed to the point $t = k/2, x = 0$ in the numerical procedure. The straightforward angle of attack is to utilize the analytical solution directly, hence defining $U(0, k/2) = u(0, k/2)$. No stable method is, however, obtained by this approach.

In order to achieve stable results, a point on the given line segment is chosen randomly, and the u-value taken at that point is assigned to the point $x = 0, t = k/2$. I.e. a uniformly distributed random variable Θ is sampled from the interval $(-1,1)$, and we define the solution at $x = 0, \quad t = k/2$ as:

$$U(0, k/2) = u(\Theta h/2, k/2) \tag{27}$$

(Hence the name Random Choice Method, also referred as the Uniform Sampling Method.)

As an example, a rarefaction solution of the Riemann problem is shown in Fig. 11. Once Θ is sampled, the numerical solution to be assigned to the point $x = 0, t = k/2$ is defined by:

$$(28)\quad U(0,k/2) = u(\Theta h/2,k/2) = \begin{cases} u_L & \text{if } \Theta h/k \leq a_L \\ u^* & \text{if } a_L < \Theta h/k < a_R \\ u_R & \text{if } \Theta h/k \geq a_R \end{cases}$$

where u^* is defined by the equation: $a(u^*) = \Theta h/k$.

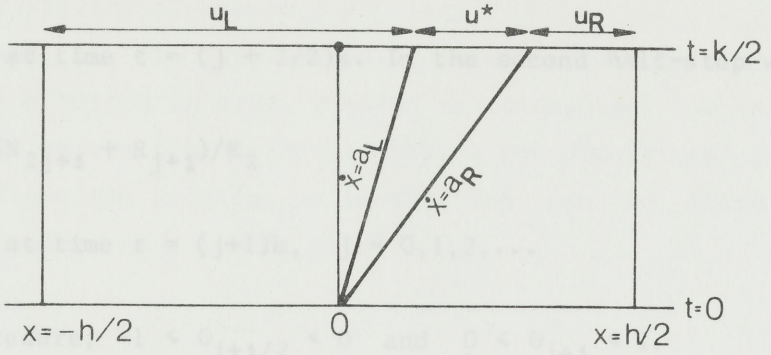

Fig. 11.

5 **The Sampling Procedure. Boundaries.**

The convergence and stability of the Random Chioce Method is sensitive to the sampling procedure, as pointed out by Chorin[1, 2]. He found that stable results were obtained only if the same value of Θ is used for every spatial point of a given time step. Θ is most naturally sampled by a pseudo random generator. We require from this generator that the Θ-distribution converges rapidly to a uniform distribution, without too small repetitive patterns, and have chosen to use a random generator proposed by Paulsen[19] that serves our purpose:

$$R_{j+1/2} \equiv 32768*R_j \pmod{16775723}, \quad j = 0, 1/2, 1, 3/2, \ldots$$

To prevent loss of information at the boundaries, Chorin suggests the following procedure:

Let $K_1 < K_2$ be mutually prime integers with K_2 odd, and let $N_1 < K_2$ be an integer. Construct the sequence of integers

(29) $N_{s+1} \equiv (N_s + K_1) \pmod{K_2}$.

Then for the Riemann problem solutions in the first half-step we use

(30) $\Theta_{j+1/2} = (N_{2j+1} + R_{j+1/2})/K_2 - 1$

when sampling at time $t = (j + 1/2)k$. In the second half-step we use

(31) $\Theta_{j+1} = (N_{2j+1} + R_{j+1})/K_2$

when sampling at time $t = (j+1)k$, $j = 0,1,2,\ldots$

With this procedure, $-1 \leq \Theta_{j+1/2} \leq 0$ and $0 \leq \Theta_{j+1} \leq 1$.

Chorin showed that boundary conditions should be treated in the following manner:
When the Dirichlet condition $u_0 = B_0$ is prescribed
we set $U\{-1/2, (j+1/2)\} = 2B_0 - U\{1/2, (j+1/2)\}$, and similar for the boundary at $x = 1$.
If we impose a Neuman condition $(\partial u/\partial n)_0 = C_0$ the image point is defined by $U\{-1/2, (j+1/2)\} = U\{1/2, (j+1/2)\} - h \cdot C_0$.

Note that this way of defining the image points may require an extension of the domain of definition for the nonlinearity function. In our study, u represents saturation, which is certainly a number between 0 and 1. $U(x = -h/2)$ as defined above may however exceed 1.
For waves travelling to the right, e.g. water displacing oil, the left-end-point condition reduces to $U(0,j) = u_0$, while the right-end condition is superfluous, as the waves travel out of the medium at this end.
If the nonlinearity function has a minimum, a(u) will be negative in some domain, and we have waves travelling to the left. In this case the last mentioned treatment of the boundary may be insufficient.

Solution of the multidimensional conservation equation demands an extension of the method which is not straightforward. One angle of attack is the "operator splitting" scheme of Sethian, Chorin, and Concus, where the problem is split into two or three one-dimensional Riemann problems which are solved sequentially. As the x-y-z components of the computed wave speeds in the different sweeps may be inconsistent with the actual displacement, an additional routine is required to analyze the propagation topology[20].
Another approach is the front tracking scheme of Glimm et al, where the Random Choice Method is used solely to determine the velocity vector of the saturation discontinuity, a one-dimensional problem. Away from the front the solution is smooth, and can be found by a finite element solver on a moving grid[13].

6 Discretization of the nonlinearity function.

The authors of the referenced papers all assume the nonlinearity function $f(u)$ to be given in a closed form. This is a valid approach e.g. for the non-viscous Burger's Equation where $f(u) = \beta u^2$. In our case, namely immiscible displacement of oil by water, the most common approach has been to define the relative permeability curves for water and oil by (u being water saturation):

$$(32) \quad k_{rw} = u^2, \qquad k_{ro} = (1-u)^2$$

Hence the nonlinearity function is:

$$(33) \quad f(u) = \frac{u^2}{u^2 + \alpha(1-u)^2} \qquad \alpha = \mu_w/\mu_o$$

This approach is less satisfactory if we wish to study a real case. A very special form of the relative permeability relationship has been assumed. This functional form will seldom or never be fulfilled in practice. Moreover, it is highly improbable that we are able to obtain any closed expression for $f(u)$ at all. The normal case is that we are given a table of measured values for relative permeabilities as a

function of saturation. Viscosity is in this discussion assumed to be constant.

We shall henceforth discuss the algorithm for the Riemann problem when f(u) is given only at a finite number of points $\{u_i, f(u_i)\}$, $i=0,1,2,\ldots,n$.

Dafermos[5] has studied the case where f(u) is a polygon-line. Our approach is, however, somewhat different. We still assume that f(u) is C^2, with known values only at selected points. The differential a(u) is computed on the node points u_i with second order accuracy. This procedure differs from Dafermos, who obtains a piecewise constant differential, while a(u) will be a discrete approximation to a continous function in our case.

Another generalization of the cases studied in the litterature hitherto, is that we permit a larger class of nonlinearity functions than previously assumed. Concus & Proskurowski[4] e.g., assume that f(u) is strictly increasing with at most one inflection point. For the time being we will allow a quite general nonlinear function, although the class of permitted fractional flow functions is restricted by physical reasoning and computational simplification later in the text.

We are concerned with the stability and convergence of the numerical procedure for the modified problem. Although the discussion is concentrated on the case of interest, namely that f(u) is approximated by a polygon-line, the argument holds equally well for an arbitrary perturbation of f(u). Hence we will show that the Riemann problem is structurally stable with respect to small perturbations of the nonlinearity function. This is an important result as f(u), the fractional flow function, always will be a result of measurements with error bounds.

We define F(u) as the polygon-line passing through the points (u_i, f_i), $i=0,1,\ldots,n$. In the same manner A(u) is defined as the polygon-line approximation to a(u). F and A are used exclusively in the procedure in place of f and a, i.e. all function values between node points are determined by linear interpolation.

6.1 **Stability analysis.**

In this section we compare the numerical solution obtained by the reference method with the "perturbed solution", achieved by using the polygon-line approximation. We denote the difference between the results obtained as the "deviation of the modified method". The main goal is to show that the discretization of the nonlinearity function is permitted if the node points are properly chosen.

The Shock Wave.

Denoting the reference results with lowercase letters, and the corresponding polygon line approximations with capital letters, we have: The shock velocity is defined by:

$$(34) \quad s = \frac{f_L - f_R}{u_L - u_R} \qquad \text{(reference)}$$

$$(35) \quad S = \frac{F_L - F_R}{u_L - u_R} \qquad \text{(perturbed)}$$

When $u_R < u_L$ the situation is shown in Fig. 12. We discuss this case in the following. The case $u_L < u_R$ is analogeous.

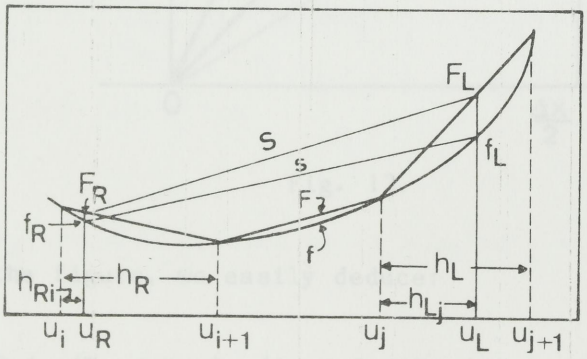

Fig. 12.

Define $T = \Delta x/\Delta t$, where Δx and Δt are the space and time increments. Then the reference solution of the Riemann problem is:

$$(36)\quad v = \begin{cases} u_R & \text{when} \quad \Theta T \geqslant s \\ u_L & \text{when} \quad \Theta T < s \end{cases}$$

while the perturbed solution is:

$$(37)\quad V = \begin{cases} u_R & \text{when} \quad \Theta T \geqslant S \\ u_L & \text{when} \quad \Theta T < S \end{cases}$$

i.e. a nonzero deviation occurs if $S < \Theta T < s$ or $s < \Theta T < S$.

We see that a deviation in the shock mode will result in a wave propagating with a shifted front velocity. We therefore discuss this case thoroughly. Symmetry considerations permit us to assume $S < s$. See Fig. 13.

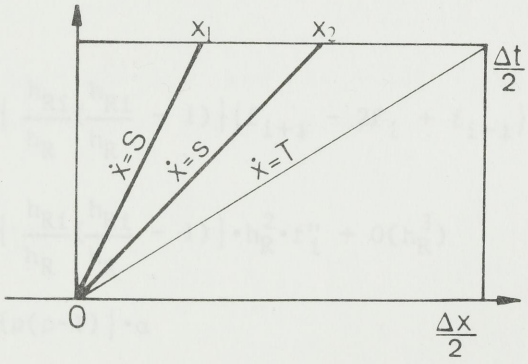

Fig. 13.

Refering to the figure, we easily deduce:

$$S/T < \Theta < s/T \iff 2x_1/\Delta x < \Theta < 2x_2/\Delta x$$

$$\iff 0 < \Theta < 2(x_2 - x_1)/\Delta x \iff 0 < \Theta < (s - S)/T$$

Hence the conditional probability that the solution is perturbed, given $S < s$ is given by: (using "PS" for "perturbed solution")

$$(38)\quad P\{\, PS \mid S < s \,\} = P\{\, S/T < \Theta < s/T \mid S < s \,\}$$
$$= P\{\, 0 < \Theta \leq (s-S)\cdot \Delta t/\Delta x \,\}$$

Define the node points u_i and u_j so that $u_i < f_R \leq u_{i+1}$ and $u_j < f_L \leq u_{j+1}$. Denote the increment $u_{i+1} - u_i$ by h_R, and similar for h_L, and let $h_{Ri} = u_R - u_i$, $h_{Lj} = u_L - u_j$.
(See Fig. 12)

We first need an expression for F_R and f_R:

$$(39)\quad F_R = f_i + h_{Ri}\frac{f_{i+1} - f_i}{h_R}$$

$$(40)\quad f_R = f_i + h_{Ri}\cdot\left\{ \frac{f_{i+1} - f_{i-1}}{2h_R} \right\} + \frac{h_{Ri}^2}{2}\left\{ \frac{f_{i+1} + f_{i-1} - 2f_i}{h_R^2} \right\} + O(h_R^3)$$

Hence

$$(41)\quad f_R - F_R = 0.5\cdot\left\{ \frac{h_{Ri}}{h_R}\left(\frac{h_{Ri}}{h_R} - 1\right)\right\}\{f_{i+1} - 2f_i + f_{i-1}\} + O(h_R^3)$$

$$= 0.5\cdot\left\{ \frac{h_{Ri}}{h_R}\left(\frac{h_{Ri}}{h_R} - 1\right)\right\}\cdot h_R^2\cdot f''_i + O(h_R^3)$$

$$\approx 0.5\cdot\{\rho(\rho-1)\}\cdot\alpha$$

where $\rho = h_{Ri}/h_R$ and α is defined by $\alpha = h_R{}^2\cdot f''_i = h_L{}^2\cdot f''_j$.

In a similar way, λ is defined by $\lambda = h_{Lj}/h_L$.
The constant α determines the increment sizes of the discretization of f(u). In short the definition states that the smallest increments should be used in regions where f changes rapidly, a conclusion which is intuitively reasonable.
From the expressions above we can calculate the difference between exact and approximate shock speed:

$$(42) \quad s-S = \frac{\{ (f_L-F_L) - (f_R-F_R) \}}{u_L - u_R} \simeq \frac{\alpha}{2(u_L-u_R)} \{\lambda(1-\lambda) - \rho(1-\rho)\}$$

The positions of u_R and u_L between two successive node points are not known, we assume that H_{Ri} and H_{Lj} will take values between 0 and H_R or H_L more or less at random. More precisely we assume that λ and ρ are uniformly distributed random variables on $[0,1]$.

Inserting Eq. (41) into Eq. (38) and rearranging gives:

$$(43) \quad P\{ PS \mid S<s \} \simeq \frac{\alpha}{2(u_L - u_R)} \frac{\Delta t}{\Delta x} \{ (1/2 - \rho)^2 - (1/2 - \lambda)^2 \}$$

Define the variables $k_R = 1/2 - \rho$ and $k_L = 1/2 - \lambda$, uniformly distributed on (-1/2, 1/2), and let

$$\beta^2 = \frac{\Delta t \cdot \alpha}{2\Delta x(u_L - u_R)}$$

Then

$$(44) \quad P\{ PS \mid S<s\} \simeq P\{ 0 < 0 \leq \beta^2 \cdot [\![k_R^2 - k_L^2]\!] \}$$

Define the random variables X and Y by:

$$(45) \quad X = \beta^2 \cdot k_R^2 \qquad Y = \beta^2 \cdot k_L^2$$

Our next task is to determine the distribution of the stochastic variables X and Y:

$$(46)\quad P\{ X \leq x \} = P\{ \beta^2 \cdot k_R^2 \leq x \} = P\{ \frac{\sqrt{x}}{\beta} \leq k_R \leq \frac{\sqrt{x}}{\beta} \} = \frac{2\sqrt{x}}{\beta}$$

where $0 \leq x \leq \frac{\beta^2}{4}$ and similar for Y.

Hence the density functions are:

$$(47)\quad f_X(x) = \frac{1}{\beta\sqrt{x}} \qquad f_Y(y) = \frac{1}{\beta\sqrt{y}}$$

A deviated solution is found if the stochastic variable $E = X-Y$ is positive and Θ is less than E. To proceed, we hence need the density function g(E) for E:

$$(48)\quad g(E) = \int_0^B f_X(y+E)\cdot f_Y(y)\, dy = \frac{1}{\beta^2} \int_0^B \frac{dy}{\sqrt{y+E}\,\sqrt{y}}$$

$$= \frac{1}{\beta^2} \log\{ \frac{\beta^2/2 - E + \beta\sqrt{\beta^2/4 - E}}{E} \}$$

where $B = \beta^2/4 - E$.

As the conditional probability $P\{ \Theta < E \mid E \}$ is simply equal to E, we have:

$$(49)\quad P\{ E > 0,\ \Theta \in (0,E) \} = \int_0^{\beta^2/4} g(E)\cdot P\{ \Theta < E \mid E \}\, dE$$

$$= \frac{\beta^2}{32} \{ 8\log(2) - \log(\beta^2) + 1/6 \}$$

The total probability that the discretization of f(u) implies a nonzero perturbation in the solution is therefore:

$$(50)\quad P\{\ PS\ \} = P\{\ PS \mid S < s\ \}\cdot P\{S < s\} + P\{\ PS \mid s < S\ \}\cdot P\{s < S\}$$

$$\simeq \frac{\Delta t}{\Delta x}\cdot\frac{\alpha}{256(u_L - u_R)}\left\{\ 8\log(2) + 1/6 - \log\left[\ \frac{\Delta t}{\Delta x}\cdot\frac{\alpha}{2(u_L - u_R)}\ \right]\right\}$$

The rarefaction wave

In the same manner as above we have the reference and approximate solutions:

$$(51)\quad v = \begin{cases} u_R & \theta T \geq a_R \\ u_L & \theta T \leq a_L \\ u^* & a_L < \theta T < a_R \end{cases}$$

$$(52)\quad V = \begin{cases} u_R & \theta T \geq A_R \\ u_L & \theta T \leq A_L \\ U^* & A_L < \theta T < A_R \end{cases}$$

where u^* and U^* are defined by $a(u^*) = A(U^*) = \theta T$

If we assume the ordering $a_L \leq A_L < a_R \leq A_R$, the situation is depicted in Fig. 14.

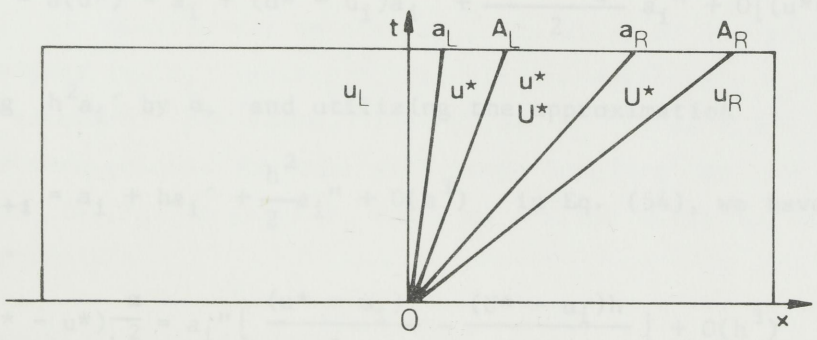

Fig. 14.

This ordering is discussed in the following, other situations are treated in a similar manner. The deviation due to the discretization of f is then:

$$(53)\quad E = \begin{cases} u_R - U^* & a_R \leqslant \Theta T \leqslant A_R \\ U^* - u^* & A_L \leqslant \Theta T \leqslant a_R \\ u_L - u^* & a_L \leqslant \Theta T \leqslant A_L \end{cases}$$

We take a(u) and A(u) as exact in the node points. (a(u) is really a second order approximation to the derivative of the nonlinearity function.)

The deviation (U* - u*) is discussed first, see Fig. 15.

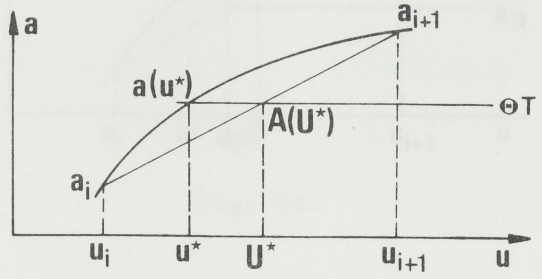

Fig. 15.

Denoting the difference $(u_{i+1} - u_i)$ by h, and using the same notation as in the previous section, we have:

$$(54)\quad \Theta T = A(U^*) = a_i + \frac{U^* - u_i}{h}(a_{i+1} - a_i) =$$

$$= a(u^*) = a_i + (u^* - u_i)a_i' + \frac{(u^* - u_i)^2}{2} a_i'' + O\left[(u^*-u_i)^3\right]$$

Replacing $h^2 a_i'$ by α, and utilizing the approximation

$$a_{i+1} = a_i + ha_i' + \frac{h^2}{2}a_i'' + O(h^3) \quad \text{in Eq. (54), we have:}$$

$$(55)\quad (U^* - u^*)\frac{\alpha}{h^2} = a_i''\left\{ \frac{(u^* - u_i)^2}{2} - \frac{(U^* - u_i)h}{2} \right\} + O(h^3)$$

Using the inequality $(u^* - u_i) \leq h$ and solving for $(U^* - u^*)$ we have

$$(56) \quad U^* - u^* \leq \frac{O(h^3)}{\frac{\alpha}{h^2} + \frac{h}{2} a_i''} = O(h^2)$$

i.e. the deviation is of the second order, and is therefore comparable with the error inherent in the numerical procedure.

From Fig. 16 we see directly that $|u_R - U^*| \leq |u^* - U^*|$ (as $a_R < \Theta T < A_R$), hence we conclude that the deviation in the rarefaction wave is always of the second order.

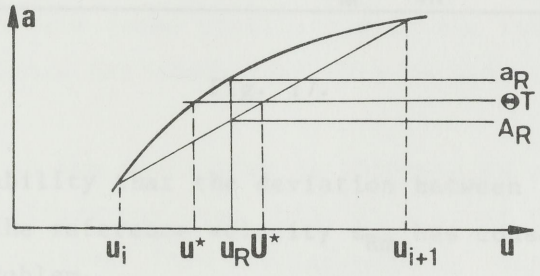

Fig. 16.

The composite wave

The solution of the Riemann problem in this case is composed by shock and rarefaction waves, the mode appointed to the numerical result hence depending on the random variable Θ. The deviation in the primitive modes is discussed above, an additional source of error is, however, introduced when we construct the convex or concave hull. As previously mentioned, the exact procedure consists of drawing a tangent from the "right" state to the curve $f = f(u)$. More precisely, the hull is constructed so that s_{Rm}, the slope of the straight line between points (u_R, f_r) and (u_m, f_m) equals the derivative $a_m = a(u_m)$. In the numerical procedure, the point u_m is searched only among candidate node points. The hull will hence be given by the straight line from (u_R, F_R) to (u_M, f_M), where u_M and the slope S_{RM} are defined by the expression

$$(57) \quad S_{RM} = \max_i \frac{f_i - F_R}{u_i - u_R} \overset{\text{def}}{===} \frac{f_M - F_R}{u_M - u_R}$$

For simplicity we set $f_R = F_R$ in the analysis. The case is shown in Fig. 17.

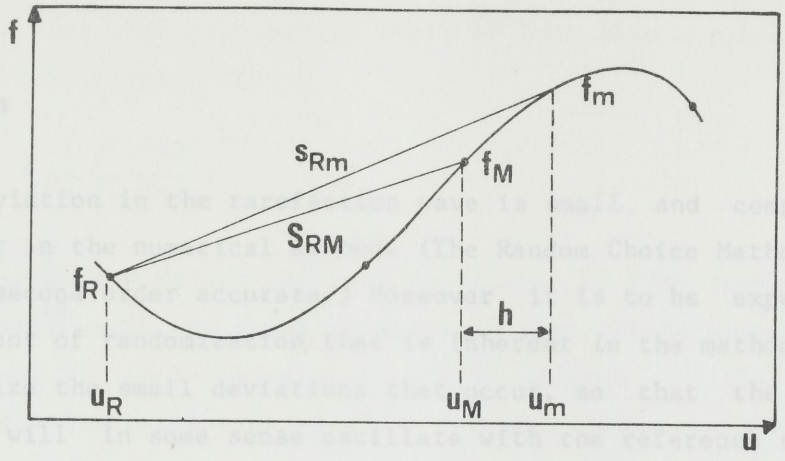

Fig. 17.

We seek the probability that the deviation between the computed shock velocity S_{RM} and the reference velocity s_{Rm} has consequences for the solution of the problem.

By definition, $s_{Rm} > S_{RM}$. Let $h = u_m - u_M$. We then have:

$$S_{RM} = \frac{f_M - f_R}{u_M - u_R} = \frac{a_m(u_m - u_R) + f_M - f_m}{u_M - u_R}$$

$$\Longrightarrow \quad a_m \left\{ \frac{u_m - u_R}{u_M - u_R} \right\} - S_{RM} = \frac{f_m - f_M}{u_M - u_R} = \frac{h \cdot a_m - h^2 a_m'/2}{u_M - u_R} + O(h^3)$$

As $a_m = \dfrac{f_m - f_R}{u_m - u_R} = s_{Rm}$ we hence have:

$$(58) \quad s_{Rm} - S_{RM} = -\frac{h^2 a_m'}{2(u_m - u_R)} = \frac{k_m^2 \cdot \alpha}{2(u_m - u_R)}$$

k_m is a uniformly distributed random variable taking values between -1 and +1. In the same manner as by the analysis following Eq. (38), it is easily shown that the probability that a nonzero deviation evolves due to the approximate construction of the hull is given by:

$$(59)\quad P\{\ PS\ \} \simeq \frac{\Delta t}{6\Delta x}\cdot\frac{\alpha}{u_m - u_R}$$

Conclusion

1. The deviation in the rarefaction wave is small and comparable to the error in the numerical method. (The Random Choice Method is close to being second order accurate.) Moreover, it is to be expected that the element of randomization that is inherent in the method will tend to stabilize the small deviations that occur, so that the perturbed solution will in some sense oscillate with the reference solution as mean value. Experience has shown that this is actually the case.

2. A perturbation in the shock wave is observed as a displacement of the shock of magnitude one grid point at a given time step, relative to the reference solution. This displacement is observed to persist for following times, and may in some instances grow larger.

Hence it is of vital interest to choose node points for the discretization of the nonlinearity function so that the probability that a perturbed shift in the shock speed occurs, is as small as possible.

We have found that the discretization process will imply a shift in the shock speed relative to the reference method with probability p. (where p is given e.g. by Eq. (50).) Define $q = 1-p$, and denote the number of shock discontinuities on a given time level by J. By elementary analysis we infer that the probability that some shock velocity is shifted at the given time step is $1-q^J$. From the analysis it is clear that a deviation can arise in <u>one</u> of the two half steps only.

After K time steps we hence have a probability q^{JK} that no shock speed deviates from the reference solution in this time interval. We therefore conclude that the probability that the first shift in the shock speed emerges during the first K time steps is given by:

$$(60)\quad P\{\text{ PS during K time steps }\} = 1 - q^{J(K-1)}$$

Demanding that this probability shall be less than a prescribed ε and solving for K, gives:

$$(61)\quad K-1 \geq \frac{\log(1-\varepsilon)}{J \cdot \log(q)}$$

By this expression we can estimate the number of time steps, and hence elapsed time, until the solution deviates from the reference solution, with a level of significance ε. As q will depend on the number of nodes in the discretization of f(u), Eq. (61) gives the number of node points necessary to obtain an acceptable solution up to time t_K, with probability $(1-\varepsilon)$.

Example.

For the fractional flow function defined by Eq. (33) the maximum value of the second derivative f"(u) is approximately 2. An appropriate average value of α is hence $\alpha = n^{-2}$, where n is the total number of discretization node points. Comparing Eqs. (50) and (59), we see that the deviation predicted by Eq.(59) is larger than the one predicted by Eq.(50) as long as n is less than approx. 100, a condition that is fulfilled in practice. Inserting the values we have utilized in our test runs, namely $\Delta x = .02$, $\Delta t = .009$, into Eq. (59) gives $p = 0.15/n^2$. This value of p is used in Eq. (61) to produce the "stability regions" shown in Fig. 18.

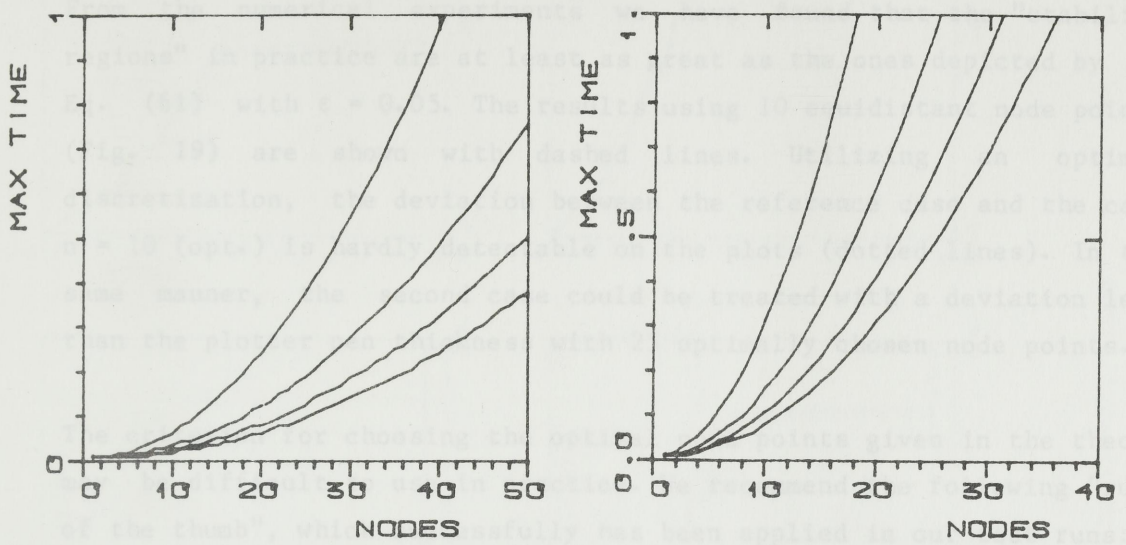

a) b)

Fig. 18.

For a given "deviation-free" time interval, the minimum number of nodes demanded is read directly from the figure. a) is for a 1% level of significance, while b) is valid for $\varepsilon = 0.05$, the value we have found to be appropriate.

Example runs are shown in Figs. 19 and 20, where the reference solution is shown with a solid line, utilizing the fractional flow function defined by Eq. (33). The dotted curves refer to results obtained using a discrete version of the same function with 10 node points.

A problem with constant initial saturation of $u = 0.05$ with boundary value $u(x=0) = 1.0$ is shown in Fig. 19, while the sequence shown in Fig. 20 has a sinusoidal initial saturation.

The first case only permits one shock to emerge, hence we use the curve $J = 1$ in Fig. 18b). With $n = 10$ we find $t_{max} = 0.315$.

This value agrees with the front curves in Fig. 19, where the first deviation in shock position is observed for $0.243 < t < 0.324$.

For the second case, $J = 3$, and in the same manner we infer that $t_{max} = 0.112$, which is in agreement with the sequence in Fig. 20.

From the numerical experiments we have found that the "stability regions" in practice are at least as great as the ones depicted by Eq. (61) with $\varepsilon = 0.05$. The results using 10 equidistant node points (Fig. 19) are shown with dashed lines. Utilizing an optimal discretization, the deviation between the reference case and the case n = 10 (opt.) is hardly detectable on the plots (dotted lines). In the same manner, the second case could be treated with a deviation less than the plotter pen thickness with 25 optimally chosen node points.

The criterion for choosing the optimal node points given in the theory may be difficult to use in practice. We recommend the following "rule of the thumb", which successfully has been applied in our test runs: Let d(i) be the maximum normal distance from F(u) to f(u) between node points u_i and u_{i+1}. The node points should be chosen so that d(i) is constant as i varies. In addition, it is advantegous to define nodes at the inflection points.

When the number of node points in the given table for the fractional flow function is insufficient, additional points may be determined by interpolation, possibly by inspection of a plotted figure. This is equally well done manually, as the qualitative look of the nonlinear function is the critical property in the procedure.

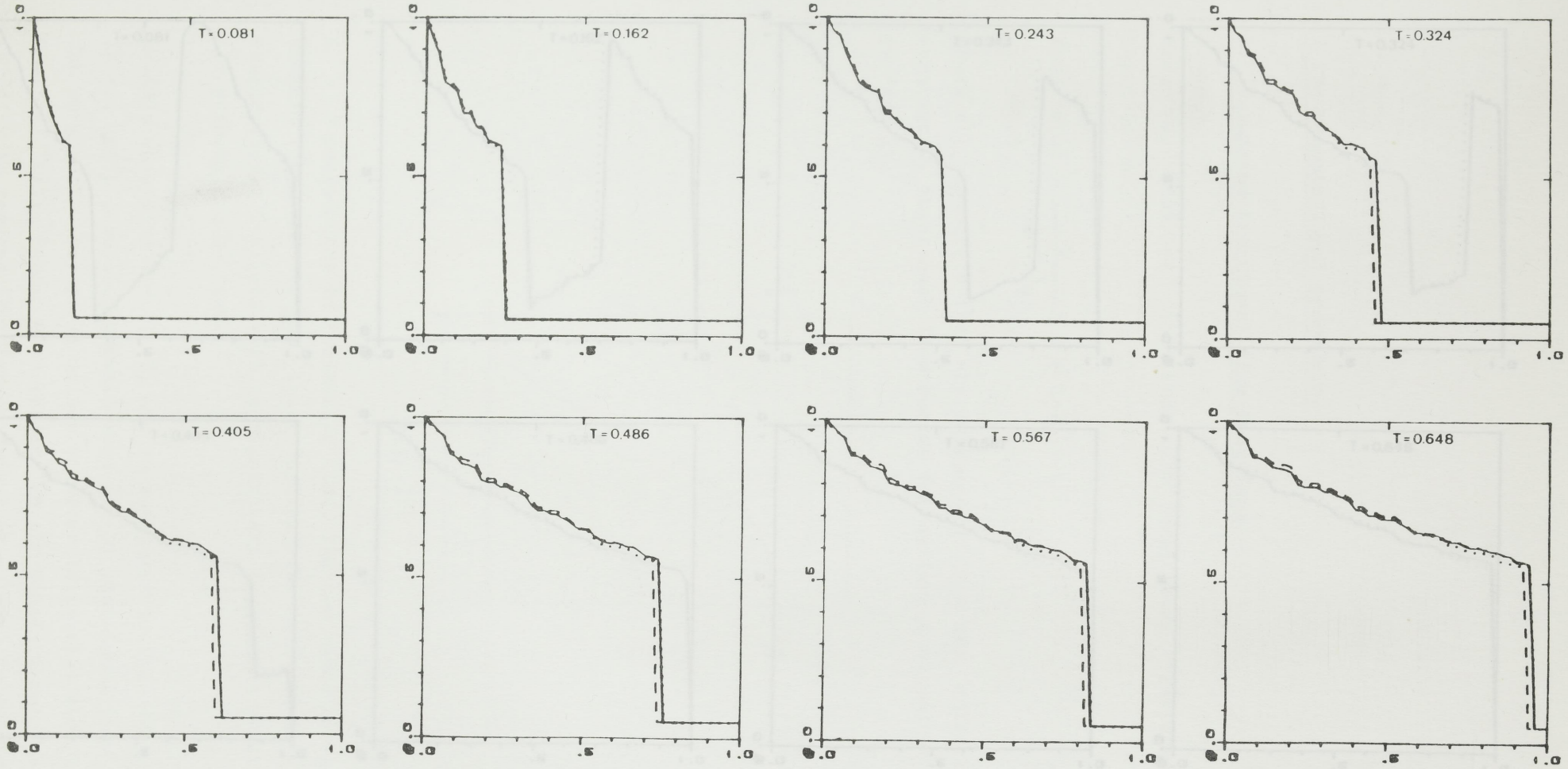

Fig. 19

Saturation distribution versus x for various (nondimensional) times
Constant initial saturation
Solid line: Reference method
Dashed line: Discrete f(u) with 10 equidistant node points
Dotted line: Discrete f(u) with 10 optimally chosen node points

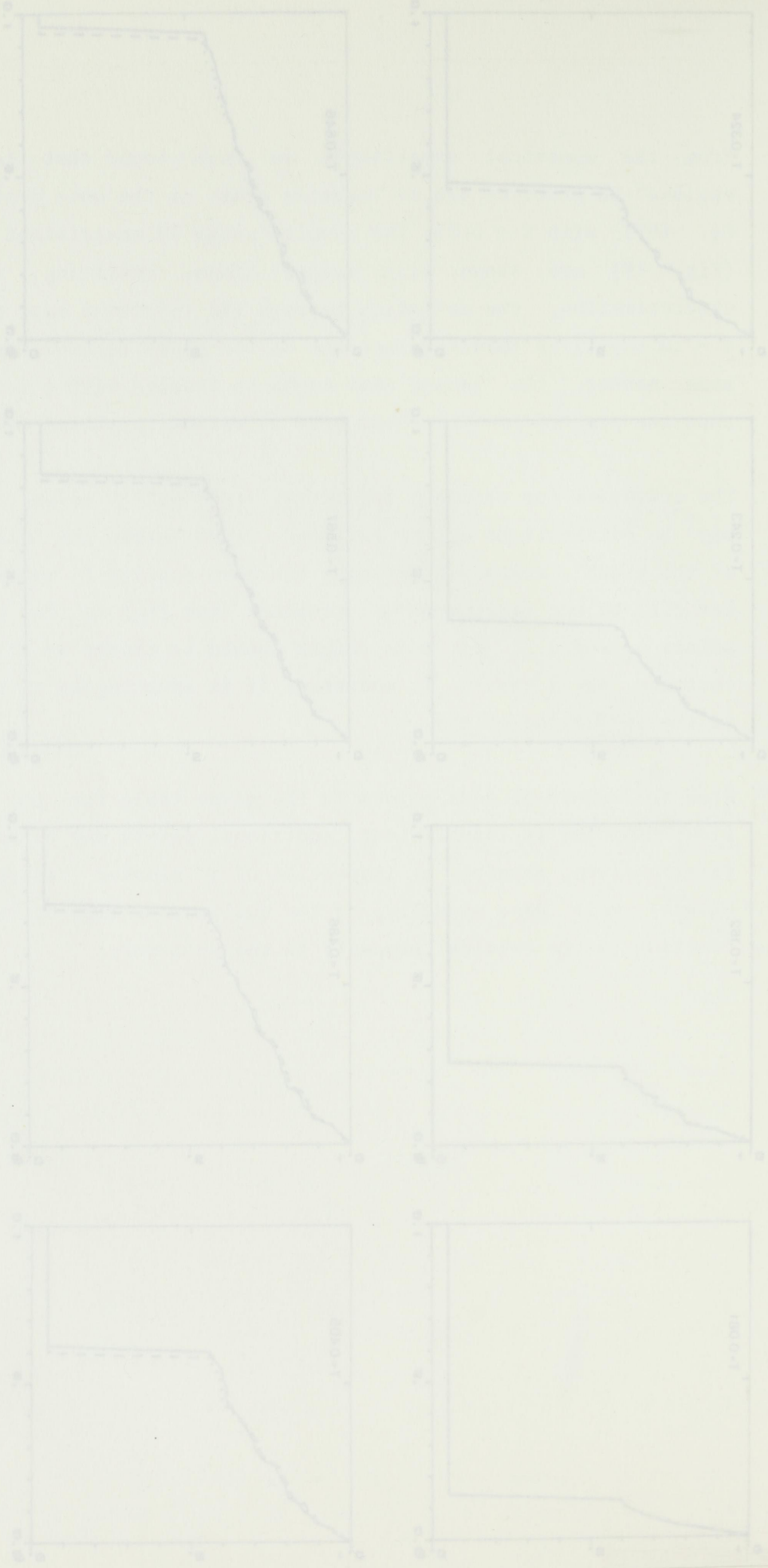

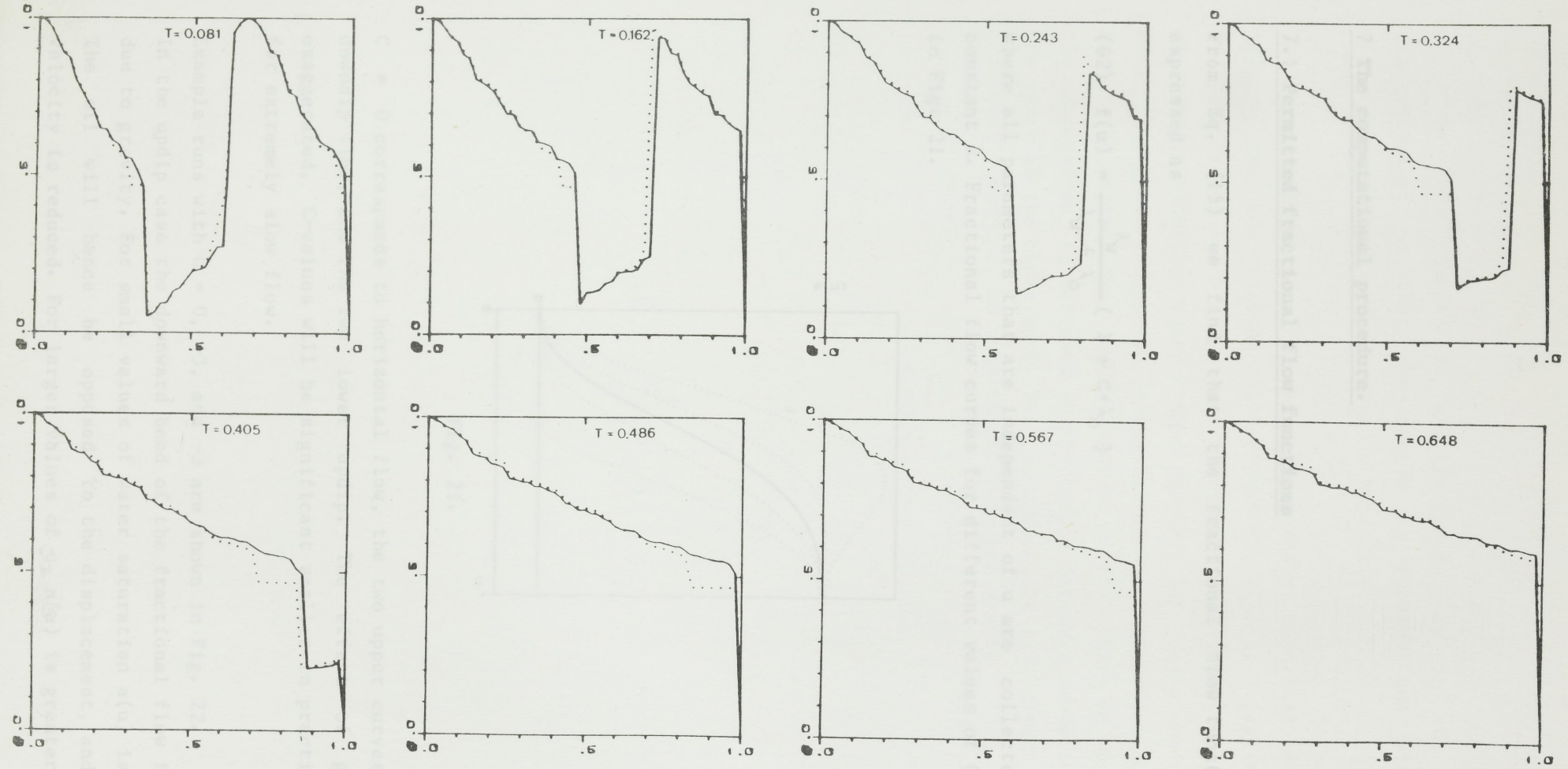

Fig. 20

Saturation distribution versus x for various (nondimensional) times
Sinusoidal initial saturation
Solid line: Reference method
Dotted line: Discrete f(u) with 10 optimally chosen node points

7 The computational procedure.

7.1 Permitted fractional flow functions

From Eq. (13) we find that the fractional flow function can be expressed as

$$(62)\quad f(u) = \frac{\lambda_w}{\lambda_w + \lambda_o}\left(1 + C\cdot\lambda_o\right)$$

where all parameters that are independent of u are collected in the constant C. Fractional flow curves for different values of C are shown in Fig. 21.

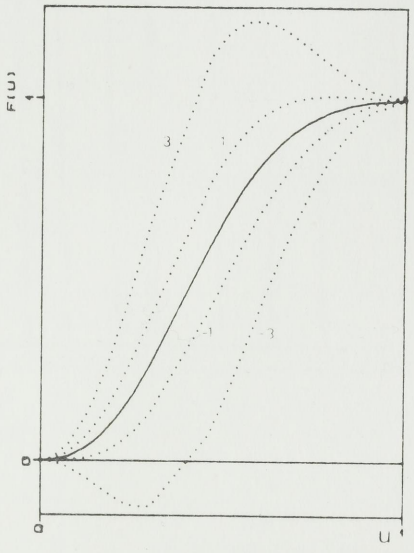

Fig. 21.

C = 0 corresponds to horizontal flow, the two upper curves represent downdip flow, and the two lower updip. The effect of gravity is exaggerated, C-values will be significant smaller in practice, except for extremely slow flow.

Example runs with C = 0, +3, and -3 are shown in Fig. 22.
In the updip case the downward bend of the fractional flow function is due to gravity. For small values of water saturation a(u) is negative. The oil will hence be opposed to the displacement, and the front velocity is reduced. For larger values of u, a(u) is greater than for

$C = 0$. This results in an increased jump in the saturation discontinuity, so that the sample is flooded out with greater efficiency. This is clearly seen in Fig. 22 b).

The upward bend of f(u) in the downdip case also results in an interval near the residual oil region where a(u) is negative. This is due to buoyancy, as a large water volume resides upon the lighter oil, an unstable situation which cannot persist. For small values of u, a(u) is increased compared to the horizontal case, which in this case results in an increased front velocity. In Fig. 22 c) we observe that the saturation is decrased to the stable interval instantaneously at the start of the experiment. The overall result is a rapid, but less efficient flood-out, an intuitively expected result.

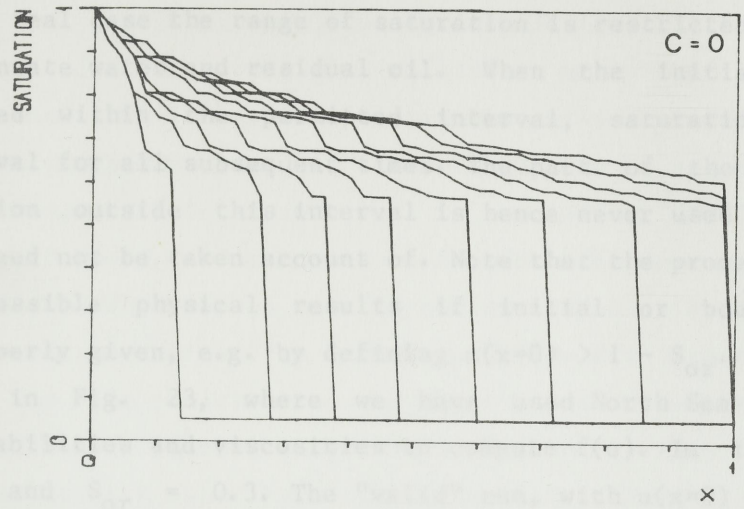
SATURATION
1
0
C = 0
0
1
x

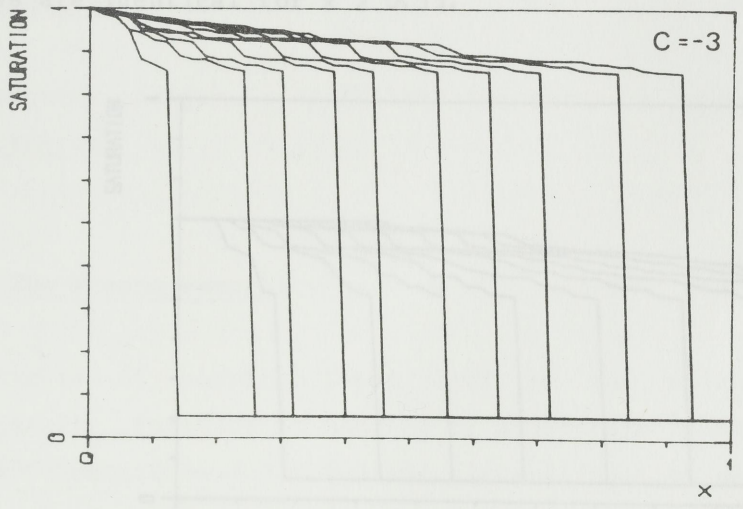
SATURATION
1
0
C = -3
0
1
x

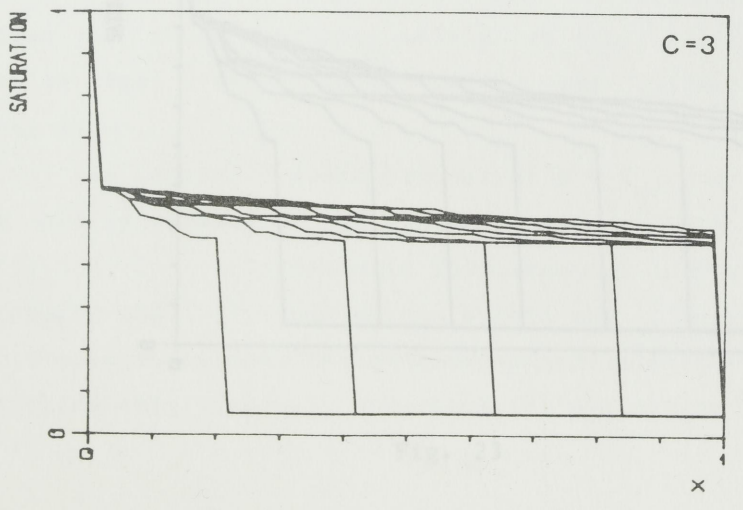
SATURATION
1
0
C = 3
0
1
x

Fig. 22

C=3

C=-3

C=0

In a real case the range of saturation is restricted by the existence of connate water and residual oil. When the initial saturation is defined within the permitted interval, saturation remains in this interval for all subsequent times. The part of the fractional flow function outside this interval is hence never used in the procedure, and need not be taken account of. Note that the procedure may produce non-possible physical results if initial or boundary values are improperly given, e.g. by defining $u(x=0) > 1 - S_{or}$. This is clearly seen in Fig. 23, where we have used North Sea data for relative permeabilities and viscosities to compute f(u). In this case $S_{wc} = 0.05$ and $S_{or} = 0.3$. The "valid" run, with $u(x=0) = 0.7$ is shown in Fig. 23 a), in b) we have put $u(x=0)$ equal to 1. Unphysical saturation values occur in the inlet end of the sample, note however that the figures are identical for $x > 0.35$.

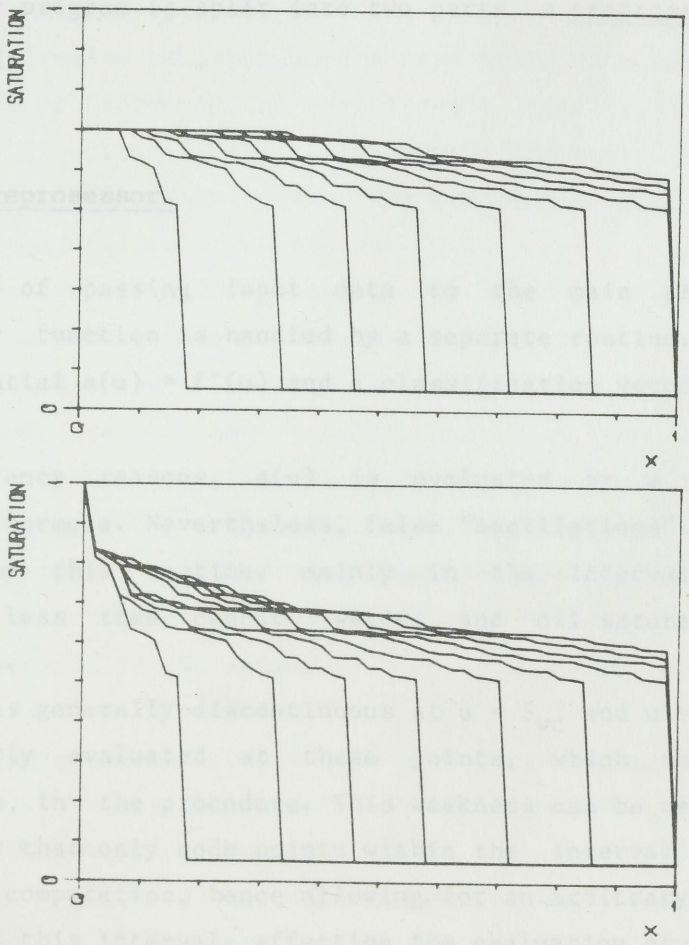

Fig. 23

From the foregoing argument we conlude that all occuring situations are covered if we permit f(u) to have at most one interior extremal point and two inflection points. This restriction is pleasant from a computational viewpoint, as the construction of a general hull (with both tangent points unknown) is avoided. This task is not at all straightforward, and may consume appreciable processor time. (See e.g. Graham[14].) Whenever a hull is constructed in the procedure, the hull will hence be a line from a known point on F(u) that touches F. To speed up the computation, the tangent points are only searched among candidate node points. As shown in the theory, this approximation is consistent with other approximations that enter the procedure.

7.2 Algorithm.

The computer program is split into two parts, a preprosessor and the main program.

7.2.1 The Preprosessor.

In advance of passing input data to the main procedure, the nonlinearity function is handled by a separate routine, which returns the differential $a(u) = f'(u)$ and a classification vector.

For consistency reasons, a(u) is evaluated by a second order difference formula. Nevertheless, false "oscillations" in f(u) may be evaluated by this routine, mainly in the intervals with water saturation less than connate water, and oil saturation less than residual oil.

As $a'(u)$ is generally discontinuous at $u = S_{wc}$ and $u = 1 - S_{or}$, a(u) may be poorly evaluated at these points, which may have great significance in the procedure. This weakness can be met by utilizing the property that only node points within the interval $[S_{wc},\ 1-S_{or}]$ enter the computation, hence allowing for an arbitrary definition of f(u) outside this interval, affecting the evaluation of a(u) only.

The classification vector is a string containing information on the inflection points of f(u), the zones where f is concave resp. convex, and indices of the u-values included in each zone.
At this point the significance of using linear interpolation when evaluating f-values between node points should be mentioned. One could a priori assume that a better algorithm could be constructed by using a higher order curve-fit to approximate f(u), e.g. a spline function. Such a procedure will inevitably introduce "false" inflection points and thereby superfluous convex/concave zones, which in turn will have a tremendous effect on the results. We use only the node values of f to construct the "classification vector", thereby guaranteeing that the correct wavetype is found for each Riemann problem. Errors introduced by the procedure will hence affect only wave speeds, not types, and the qualitative picture of the evolution is preserved.

Results from the preprosessor are written to a "metafile", which in turn is redirected as input to the next task. This can be either the main program, or normally an "analyzer", which plots the output information (f(u), a(u), inflection points and zones) for inspection. With some experience, knowledge of the fractional flow function and the initial saturation is sufficient to estimate the number of shocks that will evolve in the process. The theory then provides the appropriate number of node points in the discretization. Inspection of the preprosessor output allows one to accept the discretization and classification, reject the results and start from scratch, or most often accept the results after manually adjusting some quantities. Our experience is that a(u) frequently needs some "refreshing" in critical regions. On rarer occasions it may be desireable to move the inflection points slightly. (Superfluous or missing inflection points have never occured in our runs.)

Whether the preprosessor output data have been adjusted or not, the next stage is to use the metafile as input for the main program. The advantage with the preprosessor, aside the possibility of having influence on the handling of the nonlinearity function, is that normally a series of problems will be run with the same fractional flow function. The preprosessor is then used only prior to the first numerical experiment.

The structure of the procedure, with
preprosessor -> analyzer -> graphics output -> adjustment -> main prog, possibly skipping some of the steps, is extremely well suited for the "redirection" and "piping" facilities of the Unix operating system, in which any route we may choose among the mentioned is simply treated with a single command. Although more commands may be necessary, the structure should nevertheless easily be adapted on any system.

7.2.2 **The main program.**

The dominating part of the procedure is the calculation of the solution to the Riemann problem. For each time step a random number is drawn, and passed as argument to a sequence of calls to the procedure Riemann, one call for each grid point. The first part of this procedure classifies the configuration, determined by the positions of u_L and u_R. The configuration type (0 - 16) is passed to a procedure which evaluates the appropriate solution according to the parameters determined by the wavetype.

A flow chart for the configuration type classification is shown in Fig. 24, the 16 different nonconstant configuration types that can occur in Fig. 25, and the possible wavetypes in Fig. 26.

Abbreviations used in Fig. 24 are defined as follows:

f_R concave:	f is concave in the region surrounding f_R
$zone_R = zone_L$:	u_R and u_L lie in the same concave/convex zone
Convex hull: SRM	Construct the convex hull with slope SRM from u_R to F(u), touching F in the point u_M

"T" and "F" by the "choice-boxes" point to the appropriate route to follow, according to whether the statement in the box is true or false.

In Fig. 25 the locations of occurring inflection points are shown by solid circles. Hull tangents are drawn with a solid line when they are explicitely used in the procedure, elsewise the tangents are dashed.

Evaluation of the rarefaction wave requires the solution of a nonlinear equation $\Theta T = A(U^*)$. As A is approximated by a polygon line, this equation is explicite once the node indices on each side of the root is known. Search for particular indices also enter the routine for construction of hulls. The procedure that determines the desired nodes must hence be efficient, as it is frequently called. The search interval is first restricted by knowledge of the configuration, and the desired index is then found by binary search. The combined work to determine the appropriate index and evaluate U^* is nevertheless less time consuming than the direct solving of a nonlinear equation. Such an angle of attack is mandatory when f(u) is explicitly given, as in the reference method. In this case we use an efficient root-solver, the so-called Illinois-routine[6], a modified version of the "regula falsi" method.

8 **Conclusion.**

The Random Choice Method can be successfully applied also to cases where the fractional flow function is defined in terms of a table, if only the table values provide sufficient information on the qualitative behaviour of the displacement process. Knowledge of the physics in the model we endeavor to simulate permits the inclusion of these characteristics in the nonlinear function by manual adjustment when the given table contains an insufficient number of node points. The most general fractional flow functions occuring in practice are treated with the same ease as those studied hitherto in the litterature. Although the computer programs are more complicated than the reference programs, only small portions of the programs are used for the solution of each Riemann problem, thus the processor time is not increased. On the contrary, the test runs indicate that the discretization implies a reduction in CPU-time, as the solution of nonlinear equations is avoided.

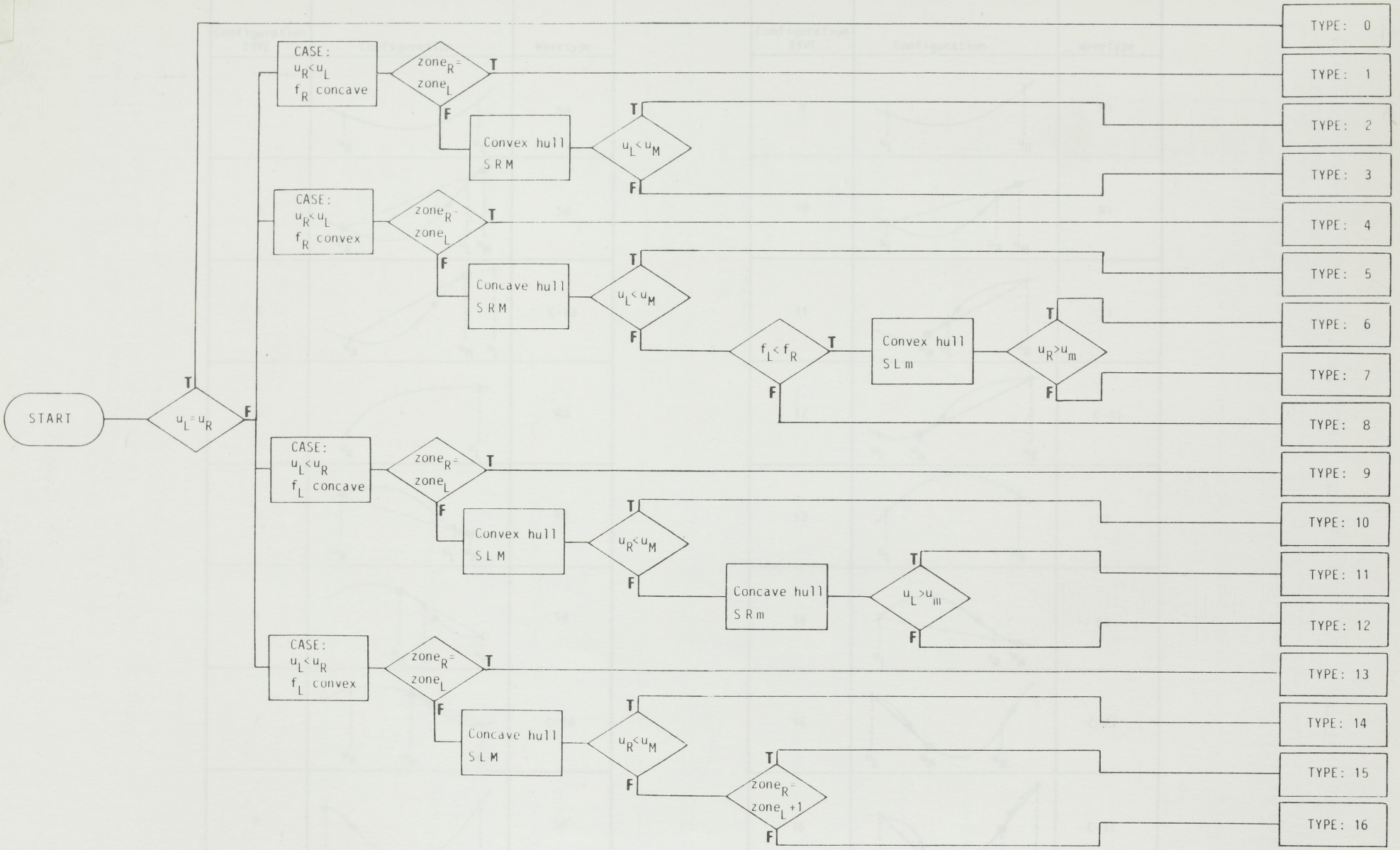
START
$u_L = u_R$
T
F
CASE:
$u_R < u_L$
f_R concave
$zone_R = zone_L$
Convex hull
S R M
$u_L < u_M$
CASE:
$u_R < u_L$
f_R convex
$zone_R = zone_L$
Concave hull
S R M
$u_L < u_M$
$f_L < f_R$
Convex hull
S L m
$u_R > u_m$
CASE:
$u_L < u_R$
f_L concave
$zone_R = zone_L$
Convex hull
S L M
$u_R < u_M$
Concave hull
S R m
$u_L > u_m$
CASE:
$u_L < u_R$
f_L convex
$zone_R = zone_L$
Concave hull
S L M
$u_R < u_M$
$zone_R = zone_L + 1$
TYPE: 0
TYPE: 1
TYPE: 2
TYPE: 3
TYPE: 4
TYPE: 5
TYPE: 6
TYPE: 7
TYPE: 8
TYPE: 9
TYPE: 10
TYPE: 11
TYPE: 12
TYPE: 13
TYPE: 14
TYPE: 15
TYPE: 16

Fig. 24

Configuration TYPE	Configuration	Wavetype
1	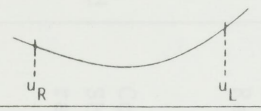	Sd
2	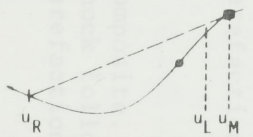	Sd
3	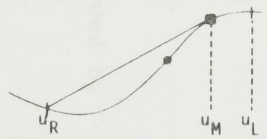	C-1d
4	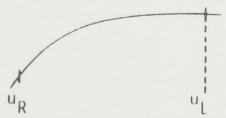	Rd
5	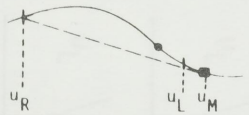	Rd
6	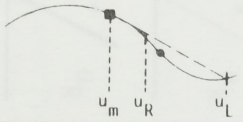	Sd
7	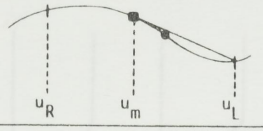	C-2d
8	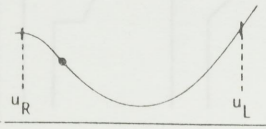	Sd

Configuration TYPE	Configuration	Wavetype
9	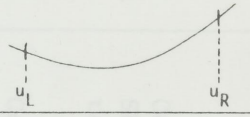	Ri
10	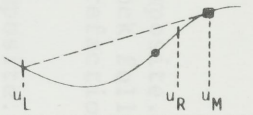	Ri
11	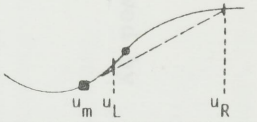	Si
12	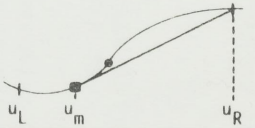	C-1i
13		Si
14	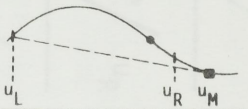	Si
15	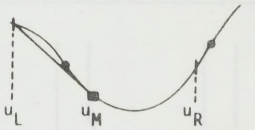	C-2i
16	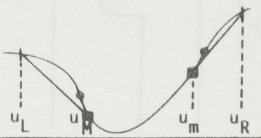	C-3i

Fig. 25

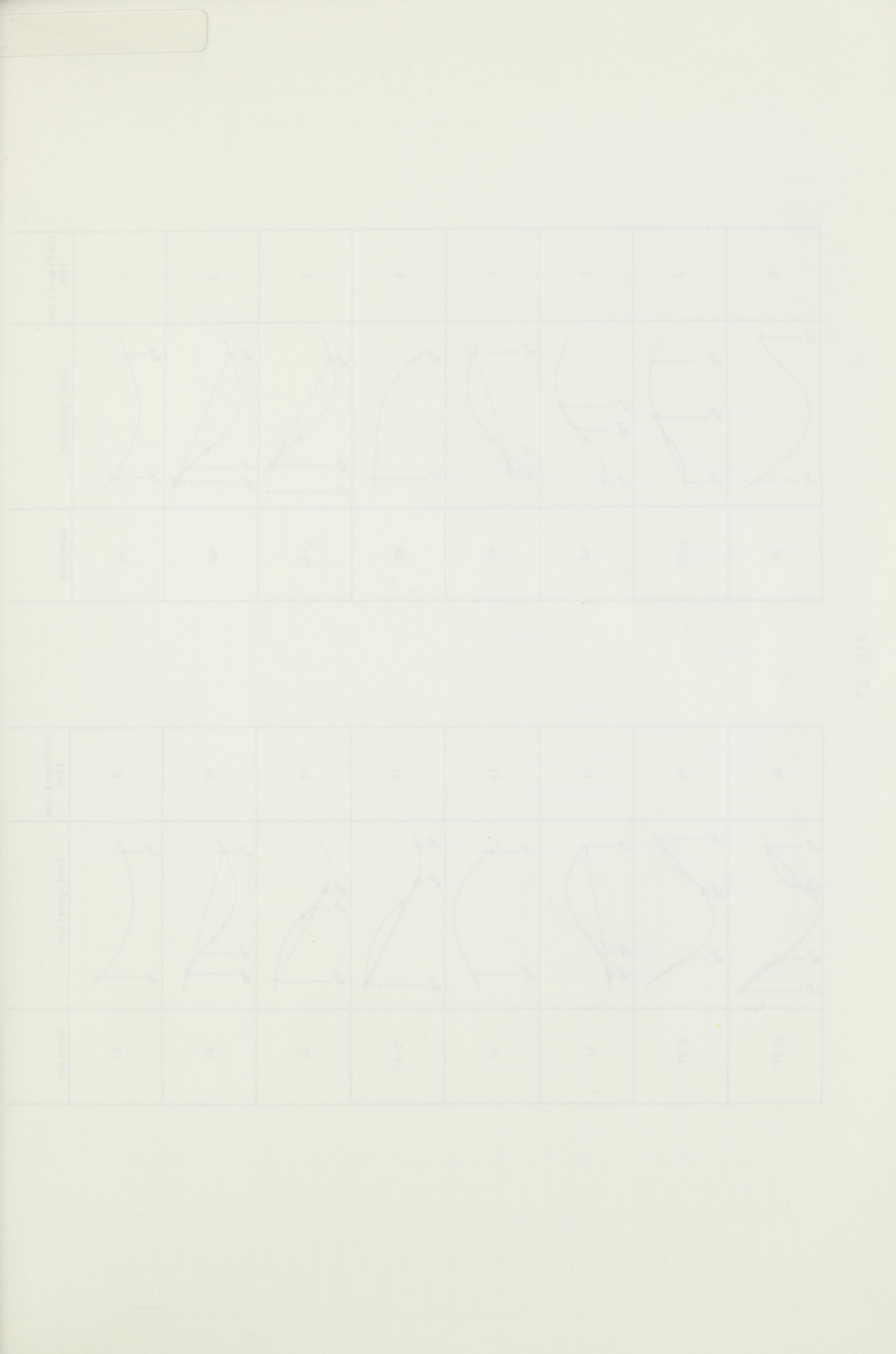

Classification of possible wave types emerging from the permitted class of fractional flow functions.

Crypt	Wave type	Pos. in x-t plan	Qualitative shape
	Increasing waves		
Si	Shock	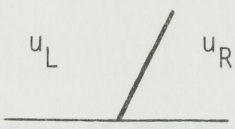	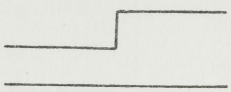
Ri	Rarefaction	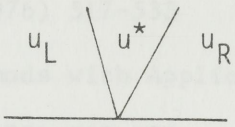	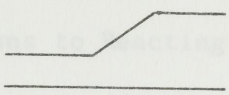
C-1i	Composite. Shock followed by rarefaction	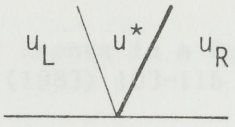	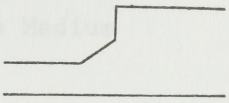
C-2i	Composite. Rarefaction followed by shock	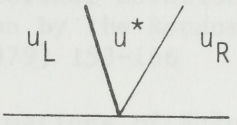	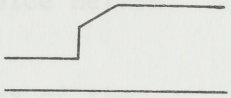
C-3i	Composite. Two shocks separated by rarefaction	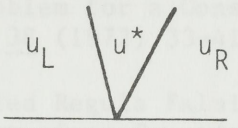	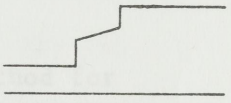
	Decreasing waves		
Sd	Shock	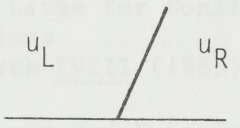	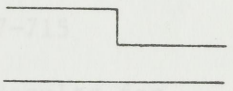
Rd	Rarefaction	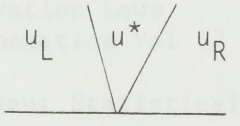	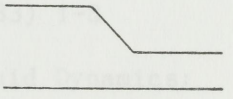
C-1d	Composite. Shock followed by rarefaction	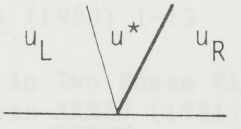	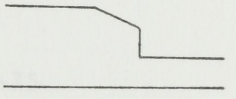
C-2d	Composite. Rarefaction followed by shock	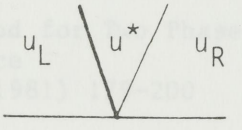	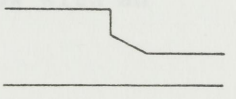

In the x-t charts a thin line represents continuous transition from a constant state into a rarefaction wave. A heavy line separates two adjacent states by a shock discontinuity.
The waves in the rightmost column are travelling to the right.

Fig. 26

Classification of possible wave types emerging from the permitted class of fractional flow functions.

Crypt	Wave type	Pos. in x-t plan	Qualitative shape
	Increasing waves		
Si	Shock		
Ri	Rarefaction		
C-1i	Composite. Shock followed by rarefaction		
C-2i	Composite. Rarefaction followed by shock		
C-3i	Composite. Two shocks separated by rarefaction		
	Decreasing waves		
Sd	Shock		
Rd	Rarefaction		
C-1d	Composite. Shock followed by rarefaction		
C-2d	Composite. Rarefaction followed by shock		

In the x-t charts a thin line represents continuous transition from a constant state into a rarefaction wave. A heavy line separates two adjacent states by a shock discontinuity.
The waves in the rightmost column are travelling to the right.

Fig. 25

References

1. A.J. Chorin: Random Choice Solution of Hyperbolic Systems
J Comp Phys 22 (1976) 517-533

2. - Random Choice Methods with Applications to Reacting Gas Flow
J Comp Phys 25 (1977) 253-272

3. - The Instability of Fronts in a Porous Medium
Comm Math Phys 91 (1983) 103-116

4. P. Concus, W. Proskurowski: Numerical Solutions of a Nonlinear Hyperbolic Equation by the Random Choice Method
J Comp Phys 30 (1979) 153-166

5. C.M. Dafermos: Polygonal Approximations of Solutions of the Initial Value Problem for a Conservation Law
J Math Anal Appl 38 (1972) 33-41

6. M. Dowell & P. Jarratt: A Modified Regula Falsi Method for Computing the Root of an Equation
BIT 11 (1971) 168-171

7. J. Glimm: Solutions in the Large for Nonlinear Hyperbolic Systems of Equations
Comm Pure Appl Math XVIII (1965) 697-715

8. - Theoretical Problems and Numerical Results for Nonlinear Conservation Laws
Contemporary Mathematics Vol 17 (1983) 1-8

9. J. Glimm, D. Marchesin, O. McBryan: Statistical Fluid Dynamics: Unstable Fingers
Comm Math Phys 74 (1980) 1-13

10. - Unstable Fingers in Two Phase Flow
Comm Pure Appl Math XXXIV (1981) 53-75

11. - A Numerical Method for Two Phase Flow with an Unstable Interface
J Comp Phys 39 (1981) 179-200

12. J. Glimm, D. Marchesin, O. McBryan, E. Isaacson:
Front Tracking for Hyperbolic Systems
Adv Appl Math 2 (1981) 91-119

13. J. Glimm, B. Lindquist, O. McBryan, B. Plohr, S. Yaniv:
Front Tracking for Petroleum Reservoir Simulation
Proc 7. SPE Symp Res Sim (1983) 41-49

14. R.L. Graham: An Efficient Algorithm for Determining the Convex Hull of a Finite Planar Set.
Inform Proc Lett 1 (1972) 132-133

15. A. Harten: The Artificial Compression Method for Computation of Shocks and Contact Discontinuities.
I. Single Conservation Law
Comm Pure Appl Math XXX (1977)

16. P. LÖtstedt: A Front Tracking Method Applied to Burger´s Equation and Two Phase Porous Flow
J Comp Phys 47 (1982) 211-228

17. O.A. Oleinik: Discontinuous Solutions of Nonlinear Differential Equations
Amer Math Soc Transl Ser 2 26 (1957) 95-172

18. - Uniqueness and a Stability of the Generalized Solution of the Cauchy Problem for a Quasilinear Equation
Amer Math Soc Transl Ser 2 33 (1964) 285-290

19. J. Paulsen: Impact of Random Number Generators in Time Series Monte Carlo Simulation
Stat Report 5 Dept Math, Univ of Bergen

20. J.A. Sethian, A.J. Chorin, P. Concus: Numerical Solution of the Buckley-Leverett Equations
Proc 7. SPE Symp Res Sim (1983) 197-204

21. J. Smoller: Shock Waves and Reaction-Diffusion Equations
Springer Verlag 1983

REPORTS PUBLISHED BY THE

DEPARTMENT OF APPLIED MATHEMATICS

UNIVERSITY OF BERGEN

BERGEN, NORWAY

No. 1. A. Kildal and S. Tjøtta.
On acoustic streaming in magneto-hydrodynamics, February 1964.

No. 2. G. Berge.
On the stability of a magnetized plasma with a continuous density force field, June 1964.

No. 3. J. Falnes.
Coaxial waveguide consisting of a circular metal tube surrounding a coaxial unidirectionally conducting sheet, August 1965.

No. 4. K.B. Dysthe.
On nonlinear interaction between two beams of plane electromagnetic waves in an anisotropic medium, December 1964.

No. 5. K.J. Overholt.
Extended Aitken acceleration, March 1965.

No. 6. G. Berge.
On the stability of a rotating plasma from the two fluid equations including finite radius of gyration effects, May 1965.

No. 7. A. Svardal.
On acoustical streaming between two coaxial cylinders, May 1965.

No. 8. K.B. Dysthe.
On convective and absolute instability, November 1965.

No. 9. L. Engevik.
On linear and non-linear hydro-magnetic vortex motion generated by the interaction of a gravity wave with a solid boundary, April 1966.

No. 10. S. Tjøtta.
Some non-linear effects in sound fields, July 1966.

No. 11. L. Engevik.
On a stability problem in hydrodynamics. Part I, November 1966.

No. 12. L. Engevik.
On the stability of plane inviscid Couette flow, November 1966.

No. 13. L. Engevik.
On a stability problem in hydrodynamics. Part II, January 1967.

Report NTNF. L. Storesletten.
On non-linear magneto-hydrodynamic wave motion in dissipative media, September 1967.

No. 14. K.B. Dysthe.
Self-trapping and self-focusing of electromagnetic waves in a plasma, May 1968.

Report no. 15 not written.

No. 16. K.B. Dysthe.
Force on a small inclusion in a standing acoustic wave, July 1968.

No. 17. A. Svardal and S. Tjøtta.
Oscillatory viscous flows in the vicinity of a cylinder, June 1969.

No. 18. A.H. Øien and J. Naze Tjøtta.
Kinetic theory of a weakly coupled and weakly inhomogeneous gas, June 1969.

No. 19. M.S. Espedal.
Hydrodynamic equations for a F.L.R. plasma, August 1969.

No. 20. J. Naze Tjøtta and A.H. Øien.
Kinetic theory of a weakly coupled and weakly inhomogeneous plasma in a magnetic field, August 1969.

No. 21. K.S. Eckhoff.
On stability.
Part I: General theory, November 1969.

No. 22. K.S. Eckhoff.
On stability.
Part II: Linear problems, December 1969.

No. 23. K.S. Eckhoff.
On stability.
Part III: The energy principle in MHD, December 1969.

No. 24. K.B. Dysthe.
On the stability of a cylindrical surface-film, December 1969.

No. 25. M.S. Espedal.
The effects of ion-ion collision on a ion-acoustic plasma pulse, April 1970.

No. 26. A.H. Øien.
Derivation of kinetic equations of a plasma using a multiple time and space scale method, September 1970.

No. 27. K.S. Eckhoff.
On stability.
Part IV: Nonlinear partial differential equations, October 1970.

No. 28. O. Faltinsen and S. Tjøtta.
Interaction between sound waves propagating in the same direction, April 1971.

No. 29. T. Leversen and J. Naze Tjøtta.
Solution of a stationary Fokker-Plank equation, June 1971.

No. 30. E. Næland.
Application of the Galerkin's method on the problem of cellular convection induced by surface tension gradients, November 1971.

No. 31. S. Nissen-Meyer.
A note on the problem of reversibility of mathematical models. (Preliminary issue.), December 1971.

No. 32. L. Hinderaker.
On the foundations of the method of matched asymptotic approximations to two meeting orthogonal boundary-layers, December 1971.

No. 33. A. Bertelsen, A. Svardal and S. Tjøtta
Non-linear streaming effects associated with oscillating cylinders, December 1971.

No. 34. S. Nissen-Meyer.
Some theorems on the problem of reversibilty of mathematical models.
(This report is a revised issue of report no. 31.), April 1972.

No. 35. I. Eidhammer.
A minimum resource sorting method, June 1972.

No. 36. T.O. Espelid.
On the behaviour of the secant method near a multiple root, September 1971.

No. 37. H.B. Drange.
The linearized Boltzmann collision operator for cut-off potentials, December 1972.

No. 38. J. Naze Tjøtta and S. Tjøtta.
Sur le transport de masse produit par des oscillations en milieu compressible, dissipatif et inhomogene, December 1972.

No. 39. M. Aksland.
On the twodimentional birth and death process with mutation, January 1973

No. 40. A. H. Øien.
Kinetic theory for evolution of a plasma in external electro-magnetic fields toward a state characterized by balance of forces transverse to the magnetic field, April 1973.

No. 41. H.B. Drange.
On the Boltzmann equation with external forces. April 1973.

No. 42. J. Naze Tjøtta and S. Tjøtta.
On the mass transport induced by time-dependent oscillations of finite amplitude in a nonhomogeneous fluid.
I General results for a perfect gas, May 1973.

No. 43. L. Engevik.
Pertubation about neutral solutions occuring in shear flows in stratified, incompressible and viscid fluids, June 1973.

No. 44. J. Naze Tjøtta and S. Tjøtta.
On the mass transport induced by time-dependent oscillations of finite amplitude in a nonhomogeneous fluid.
II General results for a liquid.
August 1973.

No. 45. G.Dahl and S. Storøy.
Enumeration of vertices in the linear programming problem, October 1973.

No. 46. M. S. Espedal.
The effects of trapped and untrapped particles on an electrostatic wave packet.
December 1973.

No. 47 M. S. Espedal.
A procedure to solve the Fokker-Planck - Poisson equations consistently, April 1974

No. 48. E. Mjølhus.
Application of the reductive perturbation method to long hydromagnetic waves parallel to the magnetic field in a cold plasma, May 1974.

No. 49. K. S. Eckhoff.
The propagation of discontinuities for linear hyperbolic partial differential equations, August 1974.

No. 50. T. O. Espelid.
An algorithm for internal merging of two subsets with small extra storage requirements, September 1974.

No. 51. E. Mæland.
Mass transport induced by wave motion in a rotating fluid, October 1974.

No. 52. I.S. Helland.
A random exchange model with constant decrements, December 1974.

No. 53. A. H. Øien.
On the evolution of a two component, two temperature, fully ionized plasma in electromagnetic fields, January 1975.

No. 54. K.S. Eckhoff.
Stability problems for linear hyperbolic systems, May 1975.

No. 55. K. S. Eckhoff.
On stability in ideal compressible hydrodynamics, May 1975.

No. 56. L. Storesletten.
A note on the stability of horizontal shear flow of an inviscid compressible fluid, July 1975.

No. 57. K. S. Eckhoff and L. Storesletten.
On the stability of shear flow in a rotating compressible and inviscid fluid, July 1975.

No. 58. E.N. Håland and C. Berge.
Dynamic stabilization of the m = 1 instability in a diffuse linear pinch, July 1975.

No. 59. E. Mæland.
Mass transport induced by wave motion in a stratified and rotating fluid, August 1975.

No. 60. T. O. Espelid.
On replacement-selection and Dinsmore's improvement, August 1975.

No. 61. L. Storesletten.
A note on the stability of steady inviscid helical gas flows, January 1976.

No. 62. E. Mæland.
A time-dependent model of coastal currents and upwelling, June 1976.

No. 63. A. H. Øien.
Corrections to classical kinetic and transport theory for a two-temperature, fully ionized plasma in electromagnetic fields, June 1977.

No. 64. S. D. Flåm.
Convergence in law of a series of φ-mixing random variables implies convergence in probability, August 1977.

No. 65. A. H. Øien.
Kinetic equation for an electron gas (non-neutral) plasma in strong fields and inhomogenities, June 1978.

No. 66. H. Hobæk and S. Tjøtta.
Theory of parametric acoustic arrays, July 1978.

No. 67. T.O. Espelid.
On floating-point summation, December 1978.

No. 68. E.N. Håland.
Stability of an inverted pendulum with hard spring and oscillating support, December 1978.

No. 69. S. Storøy.
An efficient least distance algorithm based on a general quadratic programming method, November 1979.

No. 70. L. E. Engevik.
Amplitude evolution equation for linearly unstable modes in stratified shear flows, November 1979.

No. 71. F. Oliveira-Pinto.
Argument reduction for elementary mathematical functions : An overview, July 1980.

No. 72. A. H. Øien.
A quasi moment description of the evolution of an electron gas towards a state dominated by a reduced transport equation, September 1980.

J. Berntsen.
User-documentation. Program HALF. A subroutine for numerical evaluation of three-dimensional complex integrals, spring 1983.

No. 73. S.I. Aanonsen.
Numerical computation of the nearfield of a finite amplitude sound beam, September 1983.

No. 74. L.K. Sandal.
Influence of equilibrium flows on viscous tearing modes, December 1983.

No. 75. Ø. Pettersen.
The nearfield of a high frequency amplitude shaded baffled piston. An analytical/numerical investigation, July 1981.

No. 76. Ø. Pettersen.
Numerical solution of the Buckley-Leverett equation with a general fractional flow function, November 1984.

ISSN-0084-778X

Department of Applied Mathematics
University of Bergen
Allégaten 53-55, 5000 Bergen, Norway.